Supplemental materials

MAGI1 as a link between endothelial activation and ER stress drives atherosclerosis

Jun-ichi Abe[1,8], Kyung Ae Ko[1,8], Sivareddy Kotla[1], Yin Wang[1,8], Jesus Paez-Mayorga[2,3,8], Ik Jae Shin[1,8], Masaki Imanishi[1], Hang Thi Vu[1], Yunting Tao[2], Miguel M. Leiva-Juarez[4], Tamlyn N. Thomas[1], Jan L. Medina[1], Jong Hak Won[1, 10], Yuka Fujii[1,11], Carolyn J. Giancursio[2], Elena McBeath[1], Ji-Hyun Shin[1,12], Liliana Guzman[2], Rei J. Abe[2], Jack Taunton[5], Naoki Mochizuki[6], William Faubion[7], John P. Cooke[2], Keigi Fujiwara[1,9], Scott E. Evans[4,9] and Nhat-Tu Le[2,9]

[1]Department of Cardiology, The University of Texas MD Anderson Cancer Center, Houston, TX 77030, USA.
[2]Center for Cardiovascular Regeneration, Department of Cardiovascular Sciences, Houston Methodist Research Institute, Houston TX 77030, USA.
[3]Tecnologico de Monterrey, Escuela de Medicina y Ciencias de la Salud, Monterrey, N.L., 64849, Mexico.
[4]Department of Pulmonary Medicine, The University of Texas MD Anderson Cancer Center, Houston, TX 77030, USA.
[5]Department of Cellular and Molecular Pharmacology, University of California, San Francisco, San Francisco, CA 94158, USA.
[6]Department of Cell Biology, National Cardiovascular Center Research Institute, Osaka, Japan.
[7]Division of Gastroenterology & Hepatology, Mayo Clinic, Rochester, MN 55905, USA.
[8]These authors contributed equally: Jun-ichi Abe, Kyung Ae Ko, Jesus Paez-Mayorga, Yin Wang, Ik Jae Shin.
[9]These authors were equivalent co-senior authors: Keigi Fujiwara, Scott E. Evans, Nhat-Tu Le.

Current address:
[10]Department of Obstetrics, Gynecology & Reproductive Sciences, The University of Texas Health Science Center at Houston, Houston, Texas, USA.
[11]Department of Radiology-research, Houston Methodist Research Institute, Houston TX 77030, USA.
[12]Department of Gastroenterology Hepatology & Nutrition, The University of Texas MD Anderson Cancer Center, Houston, TX 77030, USA.

Correspondence and requests for materials should be addressed to J.A. (jabe@mdanderson.org), K.F. (KFujiwara1@mdanderson.org), S.E.E. (seevans@mdanderson.org), or N.-T.L. (Nhle@houstonmethodist.org).

Running title: Unique role of MAGI1 in chronic inflammatory disease

Supplemental Methods

Antibodies and reagents

Human alpha-thrombin was purchased from Haematologic Technologies Inc. (Cat. No. HCT-0020). Recombinant human TNF was purchased from BD Biosciences (Cat. No: 554618) and Life Technologies (Cat. No. PHC 3015). Small interfering RNA (siRNA) targeting human MAGI-1 corresponding to the nucleotide 843-857 of the coding sequence (5'-GGACCCUUCUCAGAAGUUCCCUCAA)[1] was purchased from Thermo Scientific and Sigma. Anti-phospho-MAGI1-S741 was generated by Pierce Biotechnology Inc.: Rabbits were immunized with a synthesized peptide corresponding to amino acids 735 - 748 of the human MAGI1 sequence (Ac-PLERKDS*QNSSQH-C), and were checked for any adverse reactions including lesion formation, loss of appetite, and non-responsiveness. One the rabbits have passed the initial evaluation, the remaining immunization protocol was scheduled and confirmed. At the end of immunization process, the rabbits were terminated and the obtained sera were affinity purified. The entire process was performed following Pierce Biotechnology's standard protocol. All other antibodies used in this work can be found in the Supplemental Table 5. The generation of fluoromethyl ketone-methoxyethylamine (FMK-MEA) was described as previously[2]. To show the specificity of FMK-MEA, we used the Ambit/DiscoverX platform to screen 443 kinases measured the apparent binding constant (Kd) to a given inhibitor, and all kinases except RSK1/4 CTD bound with Kd >> 1 μM, suggesting that FMK-MEA is very specific to RSK1/4[3].

Magi1Gt(OST33326)Lex mice: The gene trap for Magi1Gt(OST33326)Lex mice is located between the first and second exon, closer to the 2nd exon than the first, therefore splicing out most of the first intron and inserting a STOP codon at the end of the first exon, and eliminates the full length MAGI1. We verified the depletion of MAGI1 by two different antibodies from Sigma (M5691, immunogen: amino acids 282-296 of MAGI1) and Abcam (AB37543, immunogen: C-terminus of MAGI1), which detect different sites of MAGI1.

Plasmids, and adenoviruses. An enhanced green fluorescent protein-MAGI1 construct (GenBank gene accession number KY651081) was a gift from one of the authors (N.M.)[4]. pCMV-Flag–MAGI1-WT was obtained by subcloning MAGI1 from the construct of enhanced green fluorescent protein-MAGI1 into a pCMV-Tag2B vector (Agilent Technologies) at sites recognized by the restriction enzymes *Eco*RI and *Hin*dIII. pCMV-Flag– MAGI1-S741A, MAGI1-S748A, and MAGI1-K931R mutants were generated using site-directed mutated pCMV-Flag– MAGI1-WT with a QuikChange site-directed mutagenesis kit (Agilent Technologies) according to the manufacturer's instructions. Flag-tagged adenoviral vectors containing MAGI1-WT, -S741A, and -K931R (Ad-Flag– MAGI1-WT, S741A, and K931R, respectively) were generated by cloning each corresponding insert from pCMV-Flag-MAGI1-WT, S741A, and K931R into a pENTR1A vector (Life Technologies) at sites recognized by the restriction enzymes *Kpn*I and *Not*I. The pcDNA-Myc MAGI1 fragment corresponding to amino acids 1084-1627 of MAGI1 (IFWP) was generated by cloning this fragment into a pcDNA-Myc–tagged vector at sites recognized by the restriction enzymes *Bam*HI and *Xho*I. Ad-IFWP was then generated by cloning IFWP into the pENTR1A vector at sites recognized by the restriction enzymes *Eco*RI and *Xho*I. Where indicated, an adenovirus containing β-galactosidase (Ad-LacZ) was used as a control. Plasmids containing WT-p90RSK and DN-p90RSK were described

previously[3]. A pCDN3-Rap1-N17 construct was provided by Dr. Philip Stork (Oregon Health & Science University, OR)[5].

Cells. Human umbilical vein ECs (HUVECs) were obtained from collagenase-digested umbilical cord veins[6] and collected in M200 medium supplemented with LSGS (Cascade Biologics, Inc.) and 2% FBS (Atlanta Biologicals, Inc., Lawrenceville, GA). HUVECs were cultured in 0.2% gelatin pre-coated dishes and used in experiments between 3 and 7 passages. Bovine aortic ECs (cat. no. B304-05; Cell Applications) grown in low-glucose Dulbecco's modified Eagle's medium (cat. no. SH30021.01; HyClone Laboratories) supplemented with 10% FBS and 1% P/S (100X, cat. no. 30-002-Cl; Corning) were used. The HBEC3-KT cell line was a gift from Dr. John Minna (The University of Texas Southwestern Medical Center). Mouse lung endothelial cells (MLECs) were isolated as described previously[3]. One day before cell isolation, anti-PECAM-1–conjugated Dynabeads were prepared by first conjugating the beads with sheep anti-rat IgG (cat. no. 11035; Invitrogen) and then incubating them with rat anti-mouse PECAM-1 (purified rat anti-mouse CD31, cat. no. 553370; BD Pharmingen) in a cold room overnight following the manufacturer's instructions. Whole animal perfusion was performed using phosphate-buffered saline (PBS). Lungs were harvested from the mice, washed thoroughly in cold PBS, minced finely with scissors, and digested in collagenase (2 mg/mL, cat. no. 4177; Worthington Biochemical Corporation). The resulting lung tissue suspension was triturated 15-20 times using a 20-mL syringe attached to a cannula while avoiding frothing and filtered through a cell strainer with a 70-μm pore size. The crude cell preparation was pelleted and resuspended in cold Dulbecco's PBS with Ca/Mg (cat. no. SH30264.01; HyClone Laboratories) and 0.1% bovine serum albumin (cat. no. A9576; Sigma-Aldrich). The cell suspension was then incubated with anti-PECAM-1-conjugated Dynabeads (35 μl beads/mL cell suspension) at room temperature for 30 min with end-over-end rotation. After incubation, cells bound to the beads were recovered using a magnetic separator stand (cat. no. Z5410; Promega), washed with Dulbecco's modified Eagle's medium containing 20% FBS, and suspended in a complete culture medium (Dulbecco's modified Eagle's medium containing 20% FBS supplemented with 100 μg/mL porcine heparin, 100 μg/mL EC growth supplement [cat. no. 2759; Sigma-Aldrich], minimum essential medium nonessential amino acids [cat. no. 25025Cl; Corning], 1 mM sodium pyruvate [cat. no. 15323581; Corning], and 1% P/S) and plated in 0.2% gelatin-coated Petri dishes. When the cells reached 70-80% confluence, they were detached with trypsin-ethylenediaminetetraacetic acid to generate a single-cell suspension, pelleted, resuspended in Dulbecco's PBS with Ca/Mg and 0.1% bovine serum albumin, and incubated with anti-PECAM-1–coated beads as described previously[7]. The cells bound to beads were collected, washed, cultured in a complete culture medium, and used for experiments when they became confluent. HeLa cells were maintained in Dulbecco's modified Eagle's medium supplemented with 10% FBS and 1% P/S. Human Primary Colonic Epithelial Cells (Cat. No. H-6047; Cell Biologics, Chicago, IL) were cultured in complete human Epithelial Cell growth Medium (Cat.No.221-500; Cell Applications) supplemented with 10% fetal bovine serum. Cells were maintained at 37°C with 5% CO_2. Human aortic ECs (HAECs) were a kind gift from Dr. Aldons Jake Lusis (UCLA, David Geffen School of Medicine). HUVECs and HAECs were cultured in Petri dishes or flasks coated with 0.2% gelatin type A (#901771; MP Biomedicals, Santa Ana, CA, USA), in Endothelial Cell Medium (ECM, #1001, ScienCell) containing 465 mL of basal medium, 25 mL of fetal bovine serum (FBS, #0025, ScienCell), 5 mL of Endothelial Cell Growth Supplement (ECGS, #1052, ScienCell) and 5 mL of penicillin/streptomycin solution (P/S, #0503, ScienCell).

HAECs with less than 15 passages were used in this study.

Mouse aortic vascular smooth muscle cells (VSMCs) from *Magi1*$^{+/+}$ and *Magi1*$^{-/+}$ mice were isolated by collagenase II/elastase digestion, grown in DMEM/F12 medium containing 10% fetal bovine serum, 100 units per ml penicillin and 100 μg/ml−1 streptomycin in a humidified CO_2 incubator at 37 °C and used between 3 and 5 passages[8].

Mouse splenocytes were isolated from *Magi1*$^{+/+}$ and *Magi1*$^{-/+}$ mice. In brief, after the splenocytes were released by mashing the spleen into PBS and collected, splenocytes were incubated in ACK lysis buffer (0.151m NH4Cl, 1mM. KHCO3, EDTA 0.1M). After washing the cells by PBS, the cells were cultured in RPMI 1640 medium with 10% FCS, 1% penicillin/streptomycin and 1% L-glutamine. Splenocytes number and viability was measured by using Trypan blue dye (counted the cells using Hemocytometer)[9].

Mouse peripheral blood mononuclear cells (PBMCs) were isolated from *Magi1*$^{+/+}$ and *Magi1*$^{-/+}$ mice. In brief, approximately 0.4 ml blood was collected in EDTA tubes. Dilute the blood with equal volume of PBS, then PBMCs were separated from whole blood by using density gradient centrifugation by using Histopaque-1077 at 400g at 20^0C for 30 min. The PBMC layer was removed from the tube and transferred to a new tube. After washing the cells by PBS, cells were cultured in RPMI 1640 medium with 10% FCS, 1% penicillin/streptomycin and 1% L-glutamine, at 37°C in a humidified incubator (5% CO2)[10].

Mouse bone marrow-derived macrophages (BMDMs) were isolated as described previously[11].

D-flow studies. D-flow studies were performed using a cone-and-plate apparatus as we described previously[12]. To generate d-flow, we used cones with radial grooves that were 1-mm deep. We showed tracks of fluorescent beads suspended in culture media when grooved and nongrooved cones were rotated at the same speed. Although the nongrooved cone created straight unidirectional tracks indicating steady laminar flow, tracks made by the grooved cone were short and not oriented in the same direction, indicating non-laminar (turbulent) movement of the media in the dish. Furthermore, we confirmed the ECs cell shapes under grooved cone becomes cobble stone-like shapes, also supporting that this system can recapitulate the condition observed under disturbed flow in vivo[12]. Since disturbed flow show turbulent flow pattern, we cannot calculate shear stress, which is different from the case of oscillatory flow. We used static condition as a control, because it is well known that d-flow increases inflammation, while s-flow inhibits inflammation. Therefore, if we compare the inflammatory responses in d-flow and s-flow, it is difficult to interpret whether the increase of inflammatory gene expression is due to the increase of pro-inflammatory effects by d-flow or the decrease of anti-inflammatory effects by s-flow.

***En face* staining and quantification of immunofluorescent signals.** *En face* staining of mice aorta was performed as we described previously[3,12,13]. The fluorescent intensities of images of mouse aorta were quantified using ImageJ. First, the region of interest in mice aortic arch (the entire confocal image captured at 40X from at least three different fields/animal was quantified) was selected using the selection tool on the ImageJ selection toolbar. The l-flow and d-flow areas within the aorta were identified based on the published and generally accepted anatomical locations where such flow patterns are known to occur[14-17]. First, a typical l-flow area in the greater curvature area of the aorta[15], which is also known as a high wall shear stress area, was located. Next, a d-flow area in the lesser curvature area of the aorta, which is known as a low wall shear stress area as described previously[14-17], was located. As we reported previously[13], the

EC shape outlined by anti-VE-cadherin staining was used to identify l-flow areas (elongated cell shapes) and d-flow areas (irregular cell shapes). The Color Threshold of the region of interest (Image\Adjust\Color Threshold) was adjusted. Afterward, on the Analyze menu in ImageJ, "Set Measurements" was selected, followed by selection of the field, Min & Max gray value, Integrated density, and Mean gray value. Finally, on the Analyze menu, "Measure" was selected, and the values of intensity (Integrated Density) in a popup box with a stack of values for those regions of interest were read. The same procedure was performed for a region next to the regions of interest with no fluorescence. This served as the background. The corrected total region fluorescence was calculated using the formula Integrated Density - (mean fluorescence of selected fields - background readings).

Immunostaining and quantification of nuclear translocation. ECs expressing Flag-tagged MAGI1 proteins or ECs with reduced MAGI1 expression by siRNA were quickly washed twice with cold PBS, fixed with 4% paraformaldehyde in PBS for 15 min, and permeabilized with 0.2% Triton X-100 in PBS for 10 min. Cells were then incubated with blocking buffer (5% goat serum and 0.1% NP-40 in PBS) for 60 min to block nonspecific binding and incubated with anti-Flag (cat no. 2368, Cell Signaling), anti-p90RSK (cat no.sc-231, Santa Cruz Biotechnology), or anti-ATF6 (cat no. NBP1-75478, Novus Biologicals) antibodies (1:200 dilution in 2% goat serum and 0.1% NP-40 in PBS) overnight at 4°C. Next, the cells were washed three times with PBS and incubated with Alexa Fluor 546-labeled goat anti-rabbit IgG (cat no. A-11035, 1:2000 dilution; Invitrogen), or Alex Fluor 647-labeled goat anti-rabbit IgG (1:200 dilution; cat no. 712-606-150, Jackson ImmunoResearch) for 1 h at room temperature. The cells were counterstained with DAPI to identify nuclei. The mean fluorescence in both cytosol and nuclei was measured using ImageJ, and nuclear Flag-MAGI1 translocation was assessed as a ratio of mean fluorescence in the nucleus to the mean fluorescence in cytosol greater than 1. The overlay image of DAPI and Flag-MAGI1 staining was performed using the Photoshop software (Adobe Systems). The percentage of nuclear MAGI1 or ATF6 translocation was determined by measuring the ratio of the number of nuclear translocations to the total number of cells with Flag-MAGI1 or ATF6 staining (red). The entire confocal image captured at 60X, with at least 30 cells per field for three different fields per 35-mm dish, was quantified, and the data on nuclear translocation were obtained for three to eight dishes per group.

Measurement of Pearson's correlation coefficient. Pearson's correlation coefficient was assessed by using the Colocalization Test plugin in ImageJ (http://imagej.net/mbf/colour-analysis.htm). We chose green color as channel-1, and red color as channel-2 image. This test generates a randomize image by taking random pixels from the channel-2 image, and calculates the Pearson's coefficients for channel 1 against a number of randomized channel-2 images (Rrand). Since all the values of the Pearson's correlation coefficient obtained in this study were greater than 95% of Rrand, the observed correlations were considered significant.

Transient expression of proteins. Plasmids transfection was performed by using GIBCO Opti-MEM reduced serum medium (cat. no. 31985070; Thermo Fisher Scientific) containing Plus and Lipofectamine reagents (cat. no. 11514015 and 18324020, respectively; Life Technologies) as we described previously[3].

IP and IB. Following treatment, cells were washed three times in cold PBS and lysed in 1X cell lysis buffer (cat. no. 9803S; Cell Signaling Technology) or modified RIPA buffer (50 mM Tris-HCl, pH 7.4, 150 mM NaCl, 1 mM ethylenediaminetetraacetic acid, 1% Nonidet P-40, 0.1% sodium dodecyl sulfate, 0.25% sodium deoxycholate) with a mammalian protease inhibitor cocktail (cat. no. p8340; Sigma), 1 mM phenylmethylsulfonyl fluoride (cat. no. 36978; Thermo Fisher Scientific), and 10 mM N-ethylmaleimide (cat. no. E3876; Sigma). Cell lysates were then centrifuged (21,000 x g for 15 min) to collect supernatants. Antibodies of interest were added to the obtained supernatants, and incubated overnight in a cold room, which was followed by the addition of a protein A/G agarose mixture (protein A agarose:protein G agarose at a 1:1 ratio [cat. no. 15918-014 and 15920-010, respectively; Invitrogen]). For detecting MAGI1-ATF6 binding, protein G agarose beads (cat# 10003D, Thermo Fisher) were bound with anti-Flag antibody (cat no. F3165, Sigma) or mouse IgG (cat no. I-2000, Vector) at room temperature for 20 min, and then incubated with cell lysates for 1 h. Finally, A/G or G agarose beads were washed three times in cold lysis buffer, and bound proteins in agarose beads were released in 2X sodium dodecyl sulfate sample buffer and analyzed using IB. For using automated capillary electrophoresis Western analysis, after washing the beads three times, 30 μL of 0.1M glycine pH 2.27 was added for elution, and incubated the samples for 15 min at room temperature with rocking. The eluate was neutralized by adding 30 μL of 1M Tris-Cl pH 8.0. For IB, proteins were resolved using sodium dodecyl sulfate-polyacrylamide gel electrophoresis and electrotransferred onto Hybond enhanced chemiluminescence nitrocellulose membranes (Immobilon polyvinylidene fluoride transfer membranes, cat. no. IPVH00010; EMD Millipore). The membranes were then immunoblotted with an antibody of interest[28] and then with a secondary antibody and visualized using an enhanced chemiluminescence detection reagent (cat. no. NEL105001EA; PerkinElmer). The antibodies used in this study are listed in Supplementary Table 5.

Automated Capillary electrophoresis Western analysis: Whole cell lysates were collected in modified RIPA buffer as described in the IP and IB section. A total of 5 μL of 0.4-1 mg/mL protein or 5 μL of IP eluate described above was loaded into plates and capillary electrophoresis western analysis was carried out following the manufacturer's instructions (Protein simple WES, part no. 004-600, ProteinSimple, San Jose, CA) using the 12-230 kDa Separation Module (part no. SM-W003, ProteinSimple, San Jose, CA) and either Rabbit (part no. DM-001, ProteinSimple, San Jose, CA) or Mouse (part no. DM-002, ProteinSimple, San Jose, CA) Detection Modules. Briefly, whole cell lysates were mixed with 5X fluorescent master mix containing 200 mM DTT followed by heating at 95C° for 5 min. Cell lysates, blocking buffer (antibody diluent), primary antibodies (in antibody diluent), HRP-conjugated secondary antibodies, and luminol-peroxide were then dispensed onto the separation plate. Antibodies against β-actin served as loading controls and were multiplexed with the primary antibodies for all samples. Capillary electrophoresis was performed using the instrument default settings: separation time 25 min, separation voltage 375 V, blocking 5 min, primary and secondary antibodies 30 min. Finally, automatically detected standards and peaks were manually inspected, and the data were analyzed with the inbuilt Compass software (ProteinSimple)[18].

Dynabeads® and His-Tag pulldown. HUVECs were transduced with Ad-MAGI1-wt and Ad-MAGI1-K931R separately for 24 h and then transfected with or without pCMV-sumo3-his plasmid. Cells were harvested after 24 h and cell lysates were obtained using RIPA buffer with

proteinase and phosphatase inhibitor (cat no. 78440, Thermo Fisher). His-tagged proteins were pull down by using Dynabeads® His-Tag Isolation and Pulldown cat no. 10103D, Thermo Fisher) and eluted by 500 mM Imidazole. Eluted protein were applied to run SDS-PAGE gel and SUMOlyated MAGI-1 were detected by immunoblotting with anti-Flag antibody (cat no. F3165, Sigma). Total Flag-MAGI1 and his –SUMO3 expression level also were checked by immunoblotting with anti-Flag antibody (cat no. F3165, Sigma) and anti-his antibody (cat no. 2366, Cell signaling technology).

CheckMate Mammalian Two-Hybrid System. A dual-luciferase reporter assay system (cat. no. E1960; Promega)[3,19] was used to study p90RSK-MAGI1 interaction in ECs. ECs were co-transfected with full-length murine MAGI1 (mouse MAGI1 version 1 [NM 01036]; OriGene) or human MAGI1 fused to the activation domain of VP16 (pACT-MAGI1 [murine or human]), a full-length p90RSK fused to the Gal4-binding domain (pBIND-p90RSK), and a Gal4-responsive luciferase reporter (pG5-Luc). The transfection mixture also contained Myc-IFWP or a control vector. After 24 h of transfection, cells were harvested in 1X passive lysis buffer (cat. no. E194A; Promega), and the luciferase activity in cell lysates was measured using a GloMax 20/20 Luminometer (Promega). An increase in luciferase activity, which was calculated by normalizing firefly luciferase activity according to Renilla luciferase activity (ratio of firefly luciferase activity to Renilla luciferase activity), indicates binding of p90RSK with MAGI1. Similarly, the effect of MAGI1-K931 deSUMOylation on p90RSK-ERK5 binding in the nucleus was assayed using this system. Bovine aortic ECs were transfected with a pG5-Luc vector containing five Gal4-binding sites upstream of the minimal TATA box, which is upstream of the firefly luciferase gene[3], and a combination of plasmids containing pBIND-p90RSK, pACT-ERK5-Fr (571-807)[3], MAGI1-WT, and MAGI1-K931R as indicated in Figure 6G. An increase in luciferase activity indicates binding of p90RSK with the ERK5 fragment. Negative control samples were transfected with pBIND alone.

Rap1 activation. Rap1 activity in ECs was measured using a Rap1 Activation Assay Kit (cat. no. 17-321; EMD Millipore) according to the manufacturer's instructions.

NF-κB activity assay. A mixture of a reporter gene containing five NF-κB–binding sites as an enhancer of NF-κB activity (pLuc-MCS with five repeated NF-κB–binding sites [TGGGGACTTTCCGC]; Stratagene) and a pRL-CMV vector (internal control for Renilla luciferase activity; Promega) in Reduced Serum Medium (GIBCO Opti-MEM, cat. no. 31985070; Thermo Fisher Scientific) containing DEAE-DEXTRAN (final concentration, 0.375 μg/μl, cat. no. D9885; Sigma) was transfected into ECs. Cells were then stimulated as indicated in each figure. The luciferase activity in the resulting cell lysates was then measured as described in the manufacturer instructions for the CheckMate Mammalian Two-Hybrid System and as described previously[3,19]**.**

Plasma cholesterol assay. Total cholesterol, high-density lipoprotein, LDL, and very LDL levels in mouse serum were measured using a commercially available kit (cat. no. ab65390; Abcam) according to the manufacturer's instructions.

Blood pressure measurement. Systolic blood pressure (SBP) and diastolic blood pressure (DBP) were measured by MRBP Mouse and Rat Tail Cuff Method Blood Pressure Systems

(MRBP; IITC Life Science, CA, USA). The mouse was placed in a fixator, which was then put in a heater, and the tail of mice was put through a probe. We measured at least five times and averaged them in each mice via BP Monitor software.

Measurement of mouse serum IL-6. Mouse serum IL-6 was measured by Quantikine ELISA Mouse IL-6 kit (M6000B; R&D, MN, USA) according to the manufacture's instruction.

EC apoptosis. ECs treated with siRNA were exposed to d-flow (24 h) and harvested from the dishes by incubating them with ethylenediaminetetraacetic acid (10 mM in PBS). Cells were stained with annexin V-fluorescein isothiocyanate (Annexin V-FITC Apoptosis Detection Kit, cat. no. ab14085; Abcam) according to the manufacturer's instructions. Annexin V-positive cells were quantified using a BD Accuri C6 Flow Cytometer (BD Biosciences) and the FlowJo software program.

Supplementary Information

Supplemental Figure 1. *Magi1*$^{+/-}$/*Ldlr*$^{-/-}$ and NLC/*Ldlr*$^{-/-}$ mice, and the role of MAGI1 in EC activation. (**A**) Body weights of and plasma glucose levels in *Magi1*$^{+/-}$/*Ldlr*$^{-/-}$ and NLC/*Ldlr*$^{-/-}$ mice. *Magi1*$^{+/-}$/*Ldlr*$^{-/-}$ (n = 14) and NLC/*Ldlr*$^{-/-}$ (n = 7) mice were fed an HFD for 4 weeks. Their body weights and fasting blood glucose levels measured at the indicated times are shown. The data represent mean ± SEM. n.s., not significant. (**B and C**) MAGI1 is required for expression of adhesion molecules by inflammatory stimuli in ECs. (**B and C**) HUVECs treated with control (Cont) or MAGI1 siRNA were stimulated with Thb (10 U/mL 16 h), and mRNA expression levels of MAGI1, VCAM-1, ICAM-1 (**B**), and E-selectin (**C**) were analyzed. Data are presented as mean ± SEM (n = 3). *p <0.05; **p <0.01. Statistical differences between two independent groups (**A**) were assessed using the Student t-test (two-tailed) and one-way analysis of variance followed by Bonferroni post hoc testing for multiple group (except **A**).

Supplemental Figure2. The role of MAGI1 in blood pressure and inflammation in macrophages, neutrophils, solenocytes, and vascular smooth muscle cells in *Magi1*$^{+/-}$ and *Magi1*$^{+/+}$ mice. (**A**) No difference of systolic (SBP) and diastolic blood pressure (DBP) between *Magi1*$^{+/-}$ and *Magi1*$^{+/+}$ mice. Data are presented as mean ± SEM (n = 5-6). N.S.: not significant. (**B**) No difference of serum IL-6 level between *Magi1*$^{+/-}$ (n = 6) and *Magi1*$^{+/+}$ (n = 4) mice. Data are presented as mean ± SEM. N.S.: not significant. (**C**) No difference of IL-1β mRNA expression levels in peripheral blood mononuclear cells (PBMCs), bone marrow-derived macrophages (BMDMs), spelenocytes, and vascular smooth muscle cells (VSMCs) after TNFα stimulation. Each cell was isolated from *Magi1*$^{+/-}$ and *Magi1*$^{+/+}$ mice as described in the methods and stimulated by TNFα (20 ng/ml) for 4 hrs. Statistical differences were assessed using the one-way analysis of variance followed by Bonferroni post hoc testing for multiple group. Data are presented as mean ± SEM (n = 3). N.S.: not significant. Statistical differences were assessed using the one-way analysis of variance followed by Bonferroni post hoc testing for multiple group.

Supplemental Figure 3. p90RSK-MAGI1 binding, the effect of the MAGI1-S748A mutant on p90RSK-mediated NF-κB activation, and MAGI1 deSUMOylation in ECs. (**A**) MLECs from NLC and *Magi1*$^{-/-}$ mice were stimulated with d-flow for 0-30 min,, and the expression of phosphorylated p90RSK, total p90RSK, MAGI1, and tubulin was measured via IB with antibodies specific to the proteins. Note that p90RSK activation does not depend on MAGI1. (**B**) Inhibition of murine and human MAGI1-p90RSK binding in ECs expressing IFWP according to a CheckMate Mammalian Two-Hybrid assay. The data are presented as mean ± SEM (n = 6-12). **p <0.01. (**C**) Mouse MAGI1-p90RSK binding was inhibited by IFWP in a dose-dependent manner. The dose-dependent expression of IFWP is shown in the bottom panels. The data are presented as mean ± SEM (n = 12). **p <0.01; **** p <0.0001. (**D**) HUVECs expressing pCMV-Flag MAGI1-WT or -S748A were subjected to an NF-κB activity assay in the presence or absence of p90RSK overexpression. Relative NF-κB luciferase activity in the cells was measured, and data are presented as mean ± SEM (n = 5-6). N.S., not significant. ***p <0.001. (**E**) p90RSK activation in cells with Thb-induced MAGI1 deSUMOylation. HUVECs transduced with Ad-LacZ or Ad-Flag-DN-p90RSK (MOI, 20) were exposed to Thb, and the SUMOylated MAGI1 (above the dotted line) and DN-p90RSK (below the dotted line) expression in the cells was assayed as described in Figure 5A. The data are representative of duplicate studies.

*Nonspecific band. (**F**) HAECs pretreated with FMK-MEA (10 μM, 30 min) or a vehicle were exposed to Thb (10 U/mL for the indicated times. Total cell lysates were analyzed for p90RSK, c-Jun N-terminal kinase (JNK), p38, and ERK1/2 activation using Simple Western blotting with the Wes system (Proteinsimple) with anti-p-p90RSK, -p90RSK, -p-c-Jun N-terminal kinase, -c-Jun N-terminal kinase, -p-ERK1/2, -ERK1/2, -p-p38, and -p38 antibodies as described in the methods. The data are representative of duplicate studies.

Supplemental Figure 4. MAGI1 SUMOylation in ECs detected using Myc-tagged SUMO3 and the relationship between MAGI1 phosphorylation and SUMOylation. (**A, left**) HAECs were transfected with Flag-MAGI1-WT as well as a Myc-SUMO2/3 construct. Twenty-four hours after transfection, MAGI1 SUMOylation was assessed using IP with an anti-Flag antibody followed by IB with an anti-Myc antibody (first panel above line) and then with an anti-Flag antibody to confirm that equal amounts of MAGI1 protein were pulled down (second panel above line). The bottom panels show Myc-SUMO3 expression levels in the total cell lysates. The data are representative of duplicate studies. (**A, right**) HUVECs were exposed to d-flow for 20 min, and the level of SUMOylated MAGI1 expression in them was determined via IP with an anti-MAGI1 (mouse, Santa Cruz #SS-5) antibody and then IB with an anti-SUMO2/3 antibody with capillary electrophoresis western analysis as described in the Methods. (**B-E**) MAGI1 S741 phosphorylation (**B-D**) and SUMOylation (**E**) in ECs transduced with Ad-Flag–MAGI11-WT or -K931R (**C**, **D**) or -S741A (**E**). (**B-D**) Endogenous MAGI1 expression was depleted by siRNA treatment and confirmed by Western blotting (**B**). Then, adenoviral vectors encoding MAGI1 WT or K931R mutant were transduced into MAGI1 siRNA-treated cells. Western blot results confirm Ad-Flag-MAGI1-WT and K931R mutant expression (**C**). Cells were subjected to d-flow for indicated times and MAGI1-S741 phosphorylation was assessed using capillary electrophoresis Western analysis (**D**). The panels are representatives from three different experiments. (**E**) Ad-Flag–MAGI1-WT or -S741A was co-immunoprecipitated with anti-MAGI1 followed by IB with anti-SUMO2/3. The data are representative of duplicate studies. Adenoviral transduction: MOI, 20.

Supplemental Figure 5. MAGI1-K931 deSUMOylation elicits nuclear translocation of MAGI1. Low magnification of the images shown in Figure 6A are presented. Scale bars, 20 μm

Supplemental Figure 6. Cholesterol level and reduced macrophage infiltration into the atrosclerotic plaque in *Magi1*$^{+/-}$/*Ldlr*$^{-/-}$ mice. (**A**) HDL and LDL level in NLC/*Ldlr*$^{-/-}$ and *Magi1*$^{+/-}$/*Ldlr*$^{-/-}$ mice. The data are presented as mean ± SEM (n = 6-7). (**B**) LCA and RCA sections obtained in d-flow–induced atherosclerosis studies (Figure 7A) were immunostained with antibodies against Mac3 (macrophages) or α-smooth muscle actin (smooth muscle cells). These representative immunohistochemical images of Mac3 and α-smooth muscle actin staining of atherosclerotic lesions show that macrophages infiltrate intimal lesions in the LCA but not the RCA and that macrophage infiltration is reduced in *Magi1*$^{+/-}$/*Ldlr*$^{-/-}$ mice. Scale bars, 200 μm. *We have already reported significant macrophage and foam cell accumulation in LCA lesions in the PCL model[7,20], which represents atherosclerosis formation but not restenosis of lesions (which have very limited macrophage infiltration) after angioplasty. Therefore, this figure confirms that our model is an atherosclerosis model with significant macrophage infiltration as we reported previously[21]. We randomly chose three animals from each group of NLC/*Ldlr*$^{-/-}$ and *Magi1*$^{+/-}$/*Ldlr*$^{-/-}$ mice and confirmed significant macrophage infiltration in them, especially in

NLC/*Ldlr*$^{-/-}$ mice after PCL.

Supplemental Figure 7. Co-localization of MAGI1 and macrophage staining in plaques after PCL. (**A-C**) LCA and RCA sections obtained in d-flow–induced atherosclerosis studies (Figure 7A) were stained with anti-Mac3 (macrophages, green) and anti-MAGI1 (red) and DAPI (blue). Confocal laser scanning microscopy was used to record images of the sections. Autofluorescence was not detected in the red channel. (**D**) A normal rabbit IgG was used as a negative control. Scale bars, 100 μm. (**C**) Co-localization of Mac3 and MAGI1 staining in LCA sections was assessed using Pearson's correlation coefficient as described in Methods. Data are presented as mean ± SEM. (**E** and **F**) Intensity of MAGI1 staining at the luminal surface (**E**) and medial layer (**F**) of the LCA and RCA as detected using ImageJ. Data are presented as mean ± SEM (n = 4/group). **p <0.01. N.S., not significant. (**G**) The intima:media ratios in hematoxylin- and eosin-stained LCA sections[7]. Data are presented as mean ± SEM for NLC/*Ldlr*$^{-/-}$ (n = 6) and *Magi1*$^{-/-}$/*Ldlr*$^{-/-}$ (n = 5) mice.

Supplemental Figure 8. MAGI1 expression in d-flow and l-flow areas at the murine aortic arch. (**A**) *En face* preparations of aortas from *Magi1*$^{+/+}$ mice fed an NC diet were co-immunostained with anti-VE-cadherin (green) and anti-MAGI1 (red). Shown are border areas exposed to l-flow and d-flow. (**B**) Aortas were harvested from *Magi1*$^{-/-}$ (top panel) and *Magi1*$^{+/+}$ (second and third panels from the top) mice fed an NC diet and *Magi1*$^{+/+}$/*Ldlr*$^{-/-}$ mice (fourth and fifth panels from the top) fed an HFD. *En face* preparations of the aortas were co-immunostained with anti-VE-cadherin (green) and anti-MAGI1 (red). Shown are areas exposed to l-flow and d-flow. In ECs exposed to d-flow, MAGI1 expression was increased, and it was further upregulated in early atherosclerotic lesions in *Magi1*$^{+/+}$/*Ldlr*$^{-/-}$ mice fed an HFD. The boxed areas in the fifth panel are magnified at the bottom. Scale bar, 20 μm.

Supplemental Figure 9. MAGI1 expression in human IBD samples. Paraffin-embedded sections of colonic tissues obtained from patients with ulecerative colitis or Crohn's disease and non-IBD controls were co-stained with anti-MAGI1 (red), anti-CD31 (green), and DAPI (blue). Confocal laser scanning microscopy was used to record images of the sections. Autofluorescence was not detected in the red channel. Increased MAGI1 staining at the luminal surface area was observed in these sections as shown in Figure 7g. Scale, 100 μm. Ab, antibody.

Supplemental Figure 10. Enriched disease and biological functions detected by IPA analysis and classification of differentially expressed genes regulated by MAGI1 in response to d-flow. (**A**) The expression of *Magi1* in ECs with and without d-flow after treatment with MAGI1 siRNA (siMAGI1) or control siRNA (siCont) was quantified using qRT-PCR. Data are presented as mean ± SEM (n = 3). **p <0.01. Statistical differences were assessed using the one-way analysis of variance followed by Bonferroni post hoc testing for multiple group. (**B**) Statistical significance of IPA-determined biological functions and disease gene enrichment in MAGI1 siRNA-treated ECs calculated using a right-tailed Fisher exact test and presented as -log(P) values. A larger value on the y-axis represents greater significance. We found 491 genes that were differentially expressed in MAGI1 and control siRNA-transfected cells (p <0.05; absolute fold change >2), with 386 upregulated and 105 downregulated genes in cells treated with MAGI1 siRNA. Gene expression profiles in d-flow–stimulated ECs with MAGI1 and control siRNA transfection were also analyzed using unpaired one-way analysis of variance with

a statistical threshold of $p < 0.05$ and twofold change restriction to identify differentially expressed genes in the control and *Magi1* siRNA-transfected cells stimulated by d-flow. We identified 592 genes as being differentially expressed under d-flow stimulation and classified them further based on their biological functions using Ingenuity Downstream Effects Analysis (QIAGEN). Dermatological Disease and Conditions, Immunological Disease, Antimicrobial Response, Inflammatory Response, and Infection Disease were the five most significant changes ($-\log[P] > 20$) disease and biological function categories. The *p* values, calculated using the Fisher exact test, reflects the likelihood that the association between a set of genes in our data set and a related biological function is significant. (**C**) The reduction of the "activation of granulocytes" function predicted using IPA Downstream Effect Analysis. In the Inflammatory Response category, the downstream effects analysis predicted the reduction of this function. This network displays all the genes with defined significant differential expression associated with activation of granulocytes based on published findings in the Ingenuity Knowledge Base. CCL7 and CCL2, chemokine (C-C motif) ligands 7 and 2; KIT, KIT proto-oncogene receptor tyrosine kinase; EDN1, endothelin 1; SELE, E-selectin; LGALS3BP, lectin, galactoside-binding, soluble, 3-binding protein; F2RL1, lectin, galactoside-binding, soluble, 3-binding protein (also known as PAR-2); CST3, cystatin C. Green indicates genes with decreased expression, red indicates genes with increased expression, and blue indicates a predicted decreased effect on the "activation of granulocytes" function based on published findings of a gene's effect together with a gene's expression change.

Supplemental Figure 11. Nuclear translocation of the MAGI1-ATF6 complex.
(**A**) MAGI1-ATF6 binding was assessed using a CheckMate Mammalian Two-Hybrid assay. HAECs were transfected with murine pACT-MAGI1-mouse, pBIND-ATF6, or a luciferase reporter vector (PG5-Luc), and their luciferase activity was measured. Relative MAGI1-ATF6 binding data are presented as firefly:Renilla luciferase activity ratios ($n = 11$-12). *P* value shown in figure. Data are presented as mean ± SEM. RLU, relative light units. (**B**) HUVECs were treated with ATF6 or control siRNA for 48 h and transduced with an adenovirus containing WT p90RSK (Ad -p90RSK-WT), MAGI1-WT (Ad -MAGI1-WT), or the MAGI1-K931R mutant (Ad-MAGI1-K931R). p90RSK, MAGI1, and ATF6 expression were detected using Western blotting as indicated. (**C**) HUVECs were transduced with Ad-Flag-MAGI1-WT or -K931R and then immunostained with anti-ATF6 (red) and DAPI (blue). ATF6 staining was cytoplasmic in cells transduced with Ad-Flag-MAGI1-WT but nuclear in cells transduced with Ad-Flag-MAGI1-K931R. The percentage of cellular ATF6 localization in the HUVECs is quantified in the graph at right. Data are presented as mean ± SEM. Statistical differences between two independent groups were assessed using the Student *t*-test (two-tailed).

Supplemental Table 1: Complete blood count

	(unit)	*Magi1*$^{+/+}$	*Magi1*$^{+/-}$	P value
White Blood Cells	x 10^3/µL	9.43 ± 3.18	8.02 ± 3.75	0.524
Neutrophils	x 10^3/µL	1.29 ± 1.05	0.97 ± 0.47	0.514
Lymphocytes	x 10^3/µL	7.42 ± 2.28	6.26 ± 3.33	0.526
Monocytes	x 10^3/µL	0.27 ± 0.08	0.52 ± 0.73	0.473
Eosinophils	x 10^3/µL	0.29 ± 0.19	0.4± 0.2	0.390
Basophils	x 10^3/µL	0.04 ± 0.01	0.05 ± 0.02	0.480
LUC	x 10^3/µL	0.12 ± 0.07	0.13 ± 0.06	0.788
Red Blood Cells	x 10^6/µL	9.57 ± 0.86	9.47 ± 0.28	0.787
Hemoglobin	g/dL	14.56 ± 0.36	14.38 ± 0.67	0.614
Hematocrit	%	50.68 ± 2.44	49.83 ± 1.58	0.504
Platelets	x 10^3/µL	1229.8 ± 315.66	1171.33 ± 253.8	0.741

Mean +/- SD
Student's t test

Supplemental Table 2. Demographic variables of IBD patients.

	CD	UC	Normal
n	15	15	15
Age	42.7 ± 11.38	43.5 ± 11.04	43.5 ± 11.2
Sex	F, 8/M, 7	F, 8/M, 7	F, 9/M, 6

Supplementary Table 3. Cardiovascular Disease, Organism injury and Abnormalities, Reproductive System Disease as the top ranked interaction networks based on the number of interconnected differentially expressed genes with the lowest p values based on IAP analysis as explained in the methods. (Network Score = 41, Number of Focus Molecule = 25)

Symbol	Entrez Gene Name	Exp Fold Change	Exp p-value	Exp False Discovery I	Location	Type(s)
APOL1	apolipoprotein L1	3.040	8.17E-04	1.80E-01	Extracellular Space	transporter
BTN3A1	butyrophilin subfamily 3 member A1	3.240	9.27E-04	1.82E-01	Extracellular Space	other
BTN3A2	butyrophilin subfamily 3 member A2	3.310	2.35E-03	2.43E-01	Plasma Membrane	other
BTN3A3	butyrophilin subfamily 3 member A3	3.060	1.56E-03	2.14E-01	Plasma Membrane	other
CNP	2',3'-cyclic nucleotide 3' phosphodiesterase	2.480	5.63E-03	3.24E-01	Cytoplasm	enzyme
CST3	cystatin C	2.170	3.48E-02	5.27E-01	Extracellular Space	other
CTSL	cathepsin L	2.500	1.27E-03	1.96E-01	Cytoplasm	peptidase
CXCL10	chemokine (C-X-C motif) ligand 10	28.440	9.10E-05	1.13E-01	Extracellular Space	cytokine
CXCL11	chemokine (C-X-C motif) ligand 11	26.240	2.76E-03	2.58E-01	Other	cytokine
DNAJC3	DnaJ heat shock protein family (Hsp40) member C3	-2.650	4.66E-04	1.48E-01	Cytoplasm	other
EIF2AK3	eukaryotic translation initiation factor 2 alpha kinase 3	-2.910	6.14E-03	3.31E-01	Cytoplasm	kinase
FBXO32	F-box protein 32	-2.520	3.28E-02	5.21E-01	Cytoplasm	enzyme
FKBP14	FK506 binding protein 14	-2.150	1.03E-02	3.81E-01	Cytoplasm	enzyme
H1F0	H1 histone family member 0	5.190	1.98E-03	2.26E-01	Nucleus	other
HDL	--				Plasma Membrane	complex
HYOU1	hypoxia up-regulated 1	-2.920	8.10E-05	1.13E-01	Cytoplasm	other
IgG2b	--				Other	complex
IL23	--				Extracellular Space	complex
IL17R	--				Plasma Membrane	complex
JAK	--				Cytoplasm	group
Jnk	--				Cytoplasm	group
KDELR2	KDEL endoplasmic reticulum protein retention receptor 2	-2.010	3.33E-03	2.73E-01	Cytoplasm	other
KDELR3	KDEL endoplasmic reticulum protein retention receptor 3	-2.470	7.34E-03	3.47E-01	Cytoplasm	transporter
MANF	mesencephalic astrocyte-derived neurotrophic factor	-2.200	4.64E-04	1.48E-01	Extracellular Space	other
MAP1LC3	--				Cytoplasm	group
MHC Class II (comple	--				Plasma Membrane	complex
NMI	N-myc and STAT interactor	2.700	1.27E-03	1.96E-01	Cytoplasm	transcription regulator
PRKAA	--				Cytoplasm	group
RCN3	reticulocalbin 3	-2.170	4.62E-03	3.06E-01	Cytoplasm	other
SAA	--				Nucleus	group
SLC33A1	solute carrier family 33 (acetyl-CoA transporter), member 1	-2.070	3.36E-03	2.73E-01	Cytoplasm	transporter
SPCS3	signal peptidase complex subunit 3	-2.090	1.59E-03	2.16E-01	Cytoplasm	peptidase
TNFSF15	tumor necrosis factor superfamily member 15	-13.020	4.35E-02	5.59E-01	Extracellular Space	cytokine
TXNDC5	thioredoxin domain containing 5 (endoplasmic reticulum)	-2.540	7.41E-04	1.71E-01	Cytoplasm	enzyme
XBP1	X-box binding protein 1	-2.180	5.30E-03	3.18E-01	Nucleus	transcription regulator

Supplementary Table 4. qRT-PCR primers used in the study (h = human).

Primers	Sequences
h-GAPDH-F	5'-GGT GGT CTC CTC TGA CTT CAA CA-3'
h-GAPDH-R	5'-GTT GCT GTA GCC AAA TTC GTT GT-3'
h-VCAM1-F	5'-CCG GAT TGC TGC TCA GAT TGG A-3'
h-VCAM1-R	5'-AGC GTG GAA TTG GTC CCC TCA-3'
h-ICAM1-F	5'-GTC CCC TCA AAA GTC ATC C-3'
h-ICAM1-R	5'-AAC CCC ATT CAG CGT CAC C-3'
h-Eselectin-F	5'-GCT CTG CAG CTC GGA CAT-3'
h-Eselectin-R	5'-GAA AGT CCA GCT ACC AAG GGA AT-3'
h-MAGI1-F	5'-CAT CGA CAG CTG CAA GGA G-3'
h-MAGI1-R	5'-AAT GTC GCA GGT CCT TGT TC-3'
h-spliced-XBP1-F	5′-TGC TGA GTC CGC AGC AGG TG-3′
h-spliced-XBP1-R	5′-GCT GGC AGG CTC TGG GGA AG-3′
h-XBP1-F	5'-CCT TGT AGT TGA GAA CCA GGA G-3'
h-XBP1-R	5'-GGT CCA AGT TGT CCA GAA TGC-3'
h-TNFSF15-F	5'-CTC TGC ACT GGG AAC ATG AA -3'
h-TNFSF15-R	5'-TTG GCT CAG GGT AGC TGT CT-3'
18S-F 18S-R	5'-GTA ACC CGT TGA ACC CCA TT-3' 5'-CCA TCC AAT CGG TAG TAG CG-3'
m-IL-1β-F	5'-GGG CCT CAA AGG AAA GAA TC-3'
m-IL-1β-R	5'-TAC CAG TTG GGG AAC TCT GC-3'

Supplementary Table 5. Antibodies used in the study.

Antibodies	Cat #	Vendor
RSK1 (C-21)	SC-231	Santa Cruz
VCAM1	SC-8304	Santa Cruz
ICAM1	SC-8439	Santa Cruz
MAGI1 (SS-5) MAGI1 MAGI1 (for tissue staining)	SC-100326 M5691 AB37543	Santa Cruz Sigma Abcam
Phospho-p90RSK Ser380	9341	Cell Signaling
Flag (DYKDDDDK) (binds to same epitope as Sigma's anti-Flag M2	2368	Cell Signaling
Flag	F-3165	Sigma
Tubulin	T-5168	Sigma
E-selectin	3631-100	Biovision
Rat anti-mouse PECAM-1	553370	Pharmingen
ATF6	F3165	Sigma
His	2366	Cell Signaling Technology

References

1. Sakurai, A.*, et al.* MAGI-1 is required for Rap1 activation upon cell-cell contact and for enhancement of vascular endothelial cadherin-mediated cell adhesion. *Mol Biol Cell* **17**, 966-976 (2006).
2. Cohen, M.S., Hadjivassiliou, H. & Taunton, J. A clickable inhibitor reveals context-dependent autoactivation of p90 RSK. *Nat Chem Biol* **3**, 156-160 (2007).
3. Le, N.T.*, et al.* A Crucial Role for p90RSK-Mediated Reduction of ERK5 Transcriptional Activity in Endothelial Dysfunction and Atherosclerosis. *Circulation* **127**, 486-499 (2013).
4. Sakurai, A.*, et al.* MAGI-1 is required for Rap1 activation upon cell-cell contact and for enhancement of vascular endothelial cadherin-mediated cell adhesion. *Molecular biology of the cell* **17**, 966-976 (2006).
5. Vossler, M.R.*, et al.* cAMP activates MAP kinase and Elk-1 through a B-Raf- and Rap1-dependent pathway. *Cell* **89**, 73-82 (1997).
6. Takahashi, M. & Berk, B.C. Mitogen-activated protein kinase (ERK1/2) activation by shear stress and adhesion in endothelial cells. Essential role for a herbimycin-sensitive kinase. *J Clin Invest* **98**, 2623-2631 (1996).
7. Heo, K.S.*, et al.* Disturbed flow-activated p90RSK kinase accelerates atherosclerosis by inhibiting SENP2 function. *J Clin Invest* **125**, 1299-1310 (2015).
8. Ray, J.L., Leach, R., Herbert, J.M. & Benson, M. Isolation of vascular smooth muscle cells from a single murine aorta. *Methods Cell Sci* **23**, 185-188 (2001).
9. Darroudi, F., Farooqi, Z., Benova, D. & Natarajan, A.T. The mouse splenocyte assay, an in vivo/in vitro system for biological monitoring: studies with X-rays, fission neutrons and bleomycin. *Mutat Res* **272**, 237-248 (1992).
10. Mendez-David, I.*, et al.* A method for biomarker measurements in peripheral blood mononuclear cells isolated from anxious and depressed mice: beta-arrestin 1 protein levels in depression and treatment. *Front Pharmacol* **4**, 124 (2013).
11. Singh MV, K.S., Le NT, Ko KA, Heo KS, Wang Y, Fujii Y, Vu HT, McBeath E, Thomas TN, Gi YJ, Tao Y, Medina JL, Taunton J, Carson N, Dogra V, Doyley MM, Tyrell A, Lu W, Qiu X, Stirpe NE, Gates KJ, Hurley C, Fujiwara K, Maggirwar SB, Schifitto G, and Abe J. Senescent phenotype induced by p90RSK-NRF2 signaling sensitizes monocytes and macrophages to oxidative stress in HIV+ individuals: implications for atherogenesis. . *Circulation* **in press**(2018).
12. Heo, K.S.*, et al.* PKCzeta mediates disturbed flow-induced endothelial apoptosis via p53 SUMOylation. *The Journal of cell biology* **193**, 867-884 (2011).
13. Heo, K.S., Fujiwara, K. & Abe, J. Disturbed-flow-mediated vascular reactive oxygen species induce endothelial dysfunction. *Circulation journal : official journal of the Japanese Circulation Society* **75**, 2722-2730 (2011).
14. Iiyama, K.*, et al.* Patterns of vascular cell adhesion molecule-1 and intercellular adhesion molecule-1 expression in rabbit and mouse atherosclerotic lesions and at sites predisposed to lesion formation. *Circ Res* **85**, 199-207. (1999).
15. Hajra, L.*, et al.* The NF-kappa B signal transduction pathway in aortic endothelial cells is primed for activation in regions predisposed to atherosclerotic lesion formation. *Proc Natl Acad Sci U S A* **97**, 9052-9057. (2000).
16. Jongstra-Bilen, J.*, et al.* Low-grade chronic inflammation in regions of the normal mouse arterial intima predisposed to atherosclerosis. *J Exp Med* **203**, 2073-2083 (2006).

17. Heo, K.S.*, et al.* PKCzeta mediates disturbed flow-induced endothelial apoptosis via p53 SUMOylation. *J Cell Biol* **193**, 867-884 (2011).
18. Baradaran-Heravi, A.*, et al.* Gentamicin B1 is a minor gentamicin component with major nonsense mutation suppression activity. *Proc Natl Acad Sci U S A* **114**, 3479-3484 (2017).
19. Le, N.T.*, et al.* p90RSK targets the ERK5-CHIP ubiquitin E3 ligase activity in diabetic hearts and promotes cardiac apoptosis and dysfunction. *Circ Res* **110**, 536-550 (2012).
20. Ko, K.A.*, et al.* Developing a Reliable Mouse Model for Cancer Therapy-Induced Cardiovascular Toxicity in Cancer Patients and Survivors. *Front Cardiovasc Med* **5**, 26 (2018).
21. Heo, K.*, et al.* Disturbed flow-activated p90RSK-SENP2 module accelerates atherosclerosis. *J Clin Invest* **in press**(2015).

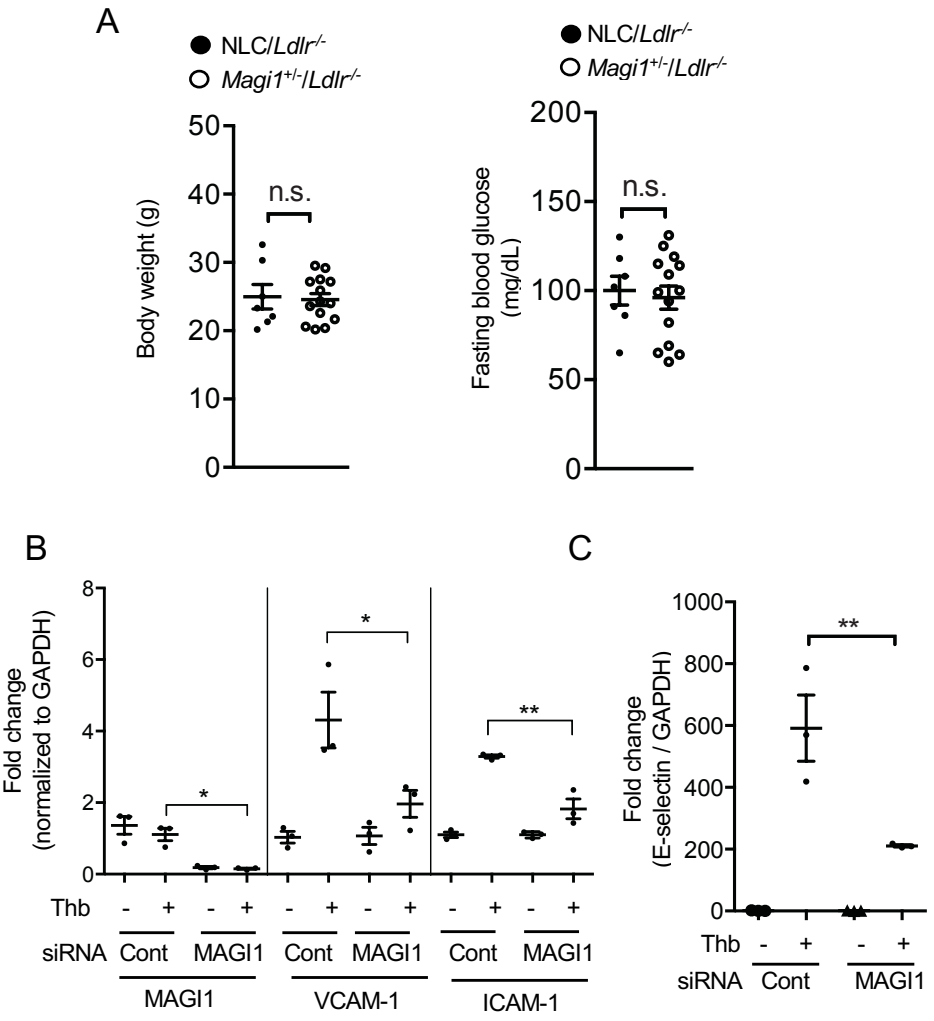

Supplemental Figure 1

Supplemental Figure 1. *Magi1*$^{+/-}$/*Ldlr*$^{-/-}$ and NLC/*Ldlr*$^{-/-}$ mice, and the role of MAGI1 in EC activation. (**A**) Body weights of and plasma glucose levels in *Magi1*$^{+/-}$/*Ldlr*$^{-/-}$ and NLC/*Ldlr*$^{-/-}$ mice. *Magi1*$^{+/-}$/*Ldlr*$^{-/-}$ (n = 14) and NLC/*Ldlr*$^{-/-}$ (n = 7) mice were fed an HFD for 4 weeks. Their body weights and fasting blood glucose levels measured at the indicated times are shown. The data represent mean ± SEM. n.s., not significant. (**B and C**) MAGI1 is required for expression of adhesion molecules by inflammatory stimuli in ECs. (**B and C**) HUVECs treated with control (Cont) or MAGI1 siRNA were stimulated with Thb (10 U/mL 16 h), and mRNA expression levels of MAGI1, VCAM-1, ICAM-1 (**B**), and E-selectin (**C**) were analyzed. Data are presented as mean ± SEM (n = 3). *p <0.05; **p <0.01. Statistical differences between two independent groups (**A**) were assessed using the Student t-test (two-tailed) and one-way analysis of variance followed by Bonferroni post hoc testing for multiple group (except **A**).

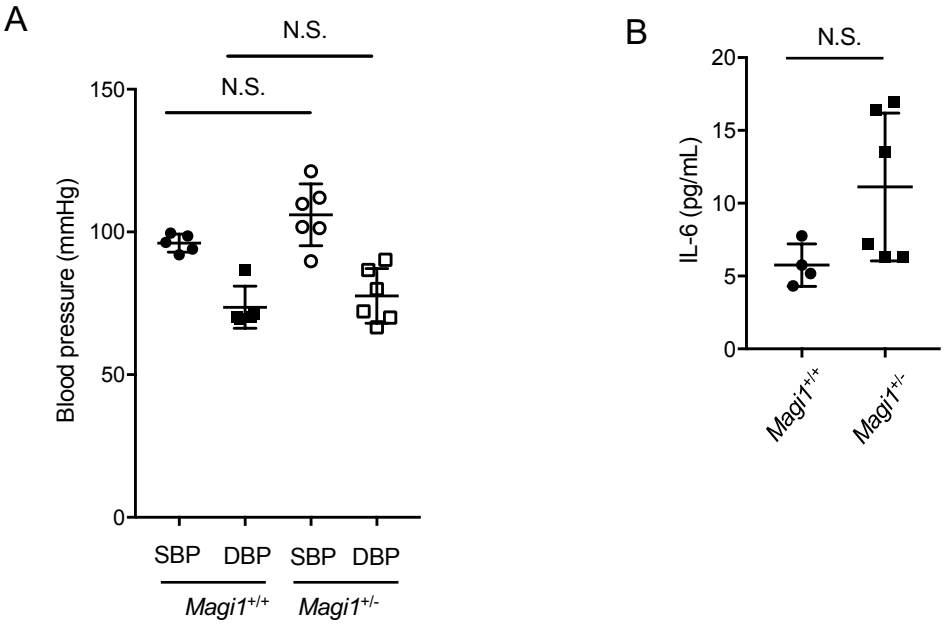

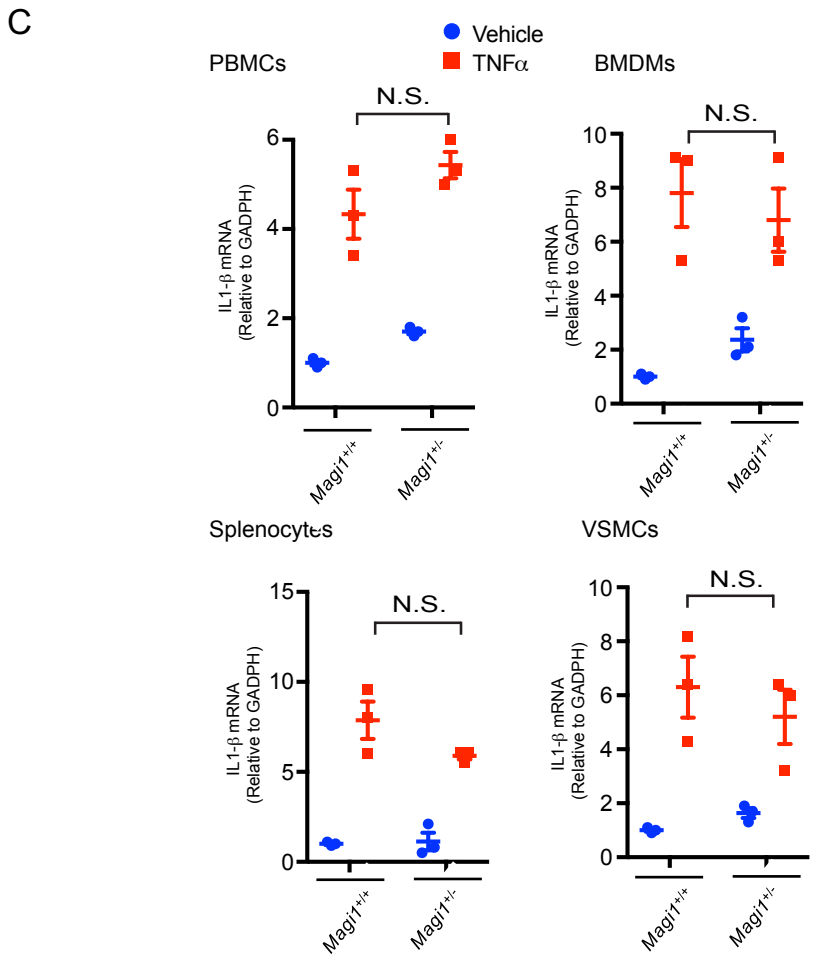

Supplemental Figure 2

Supplemental Figure2. The role of MAGI1 in blood pressure and inflammation in macrophages, neutrophils, solenocytes, and vascular smooth muscle cells in *Magi1*$^{+/-}$ and *Magi1*$^{+/+}$ mice. (**A**) No difference of systolic (SBP) and diastolic blood pressure (DBP) between *Magi1*$^{+/-}$ and *Magi1*$^{+/+}$ mice. Data are presented as mean ± SEM (*n* = 5-6). N.S.: not significant. (**B**) No difference of serum IL-6 level between *Magi1*$^{+/-}$ (n = 6) and *Magi1*$^{+/+}$ (n = 4) mice. Data are presented as mean ± SEM. N.S.: not significant. (**C**) No difference of IL-1β mRNA expression levels in peripheral blood mononuclear cells (PBMCs), bone marrow-derived macrophages (BMDMs), spelenocytes, and vascular smooth muscle cells (VSMCs) after TNFα stimulation. Each cell was isolated from *Magi1*$^{+/-}$ and *Magi1*$^{+/+}$ mice as described in the methods and stimulated by TNFα (20 ng/ml) for 4 hrs. Statistical differences were assessed using the one-way analysis of variance followed by Bonferroni post hoc testing for multiple group. Data are presented as mean ± SEM (*n* = 3). N.S.: not significant. Statistical differences were assessed using the one-way analysis of variance followed by Bonferroni post hoc testing for multiple group.

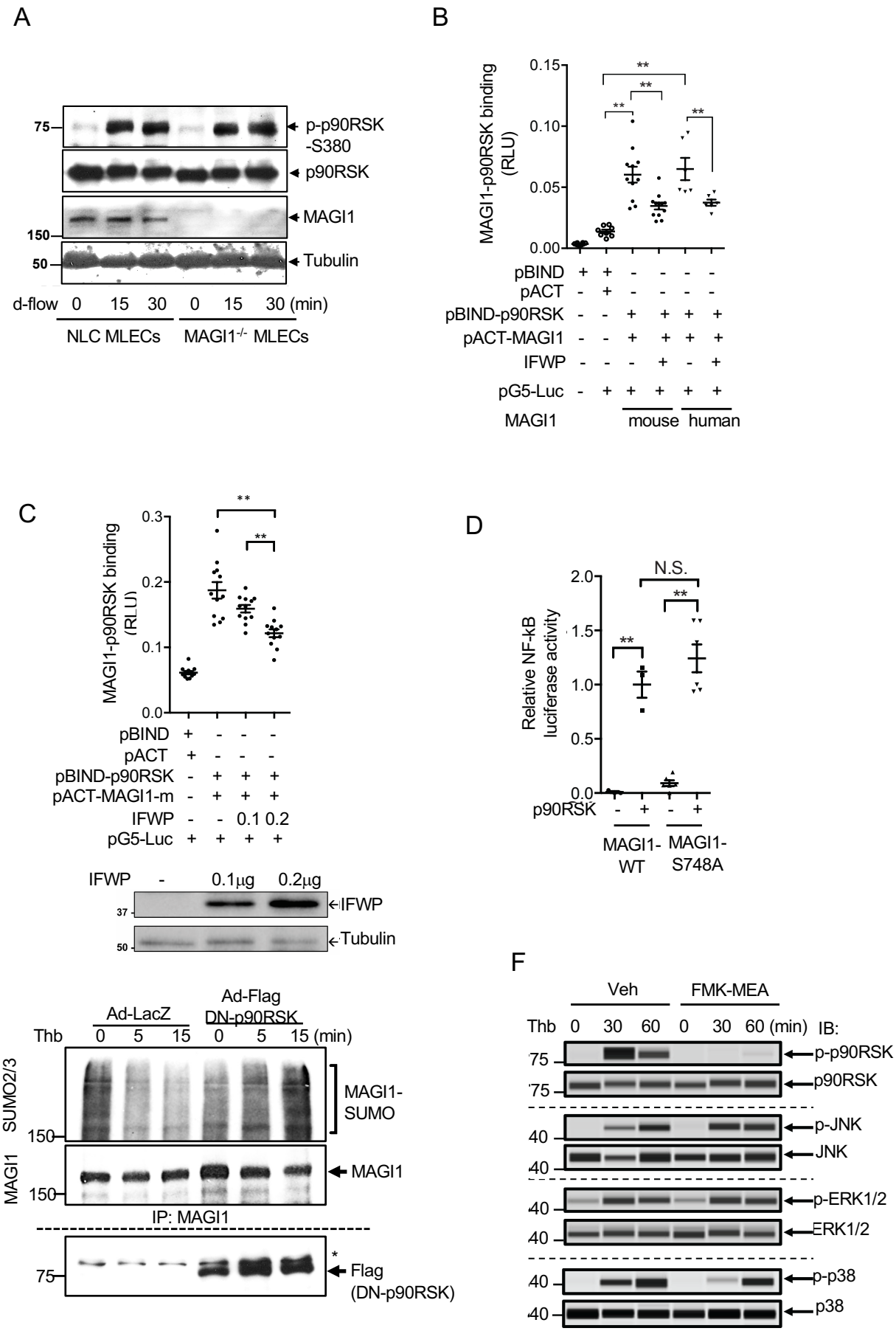

Supplemental Figure 3

Supplemental Figure 3. p90RSK-MAGI1 binding, the effect of the MAGI1-S748A mutant on p90RSK-mediated NF-κB activation, and MAGI1 deSUMOylation in ECs. (**A**) MLECs from NLC and *Magi1*$^{-/-}$ mice were stimulated with d-flow for 0-30 min,, and the expression of phosphorylated p90RSK, total p90RSK, MAGI1, and tubulin was measured via IB with antibodies specific to the proteins. Note that p90RSK activation does not depend on MAGI1. (**B**) Inhibition of murine and human MAGI1-p90RSK binding in ECs expressing IFWP according to a CheckMate Mammalian Two-Hybrid assay. The data are presented as mean ± SEM (n = 6-12). **p <0.01. (**C**) Mouse MAGI1-p90RSK binding was inhibited by IFWP in a dose-dependent manner. The dose-dependent expression of IFWP is shown in the bottom panels. The data are presented as mean ± SEM (n = 12). **p <0.01; **** p <0.0001. (**D**) HUVECs expressing pCMV-Flag MAGI1-WT or -S748A were subjected to an NF-κB activity assay in the presence or absence of p90RSK overexpression. Relative NF-κB luciferase activity in the cells was measured, and data are presented as mean ± SEM (n = 5-6). N.S., not significant. ***p <0.001. (**E**) p90RSK activation in cells with Thb-induced MAGI1 deSUMOylation. HUVECs transduced with Ad-LacZ or Ad-Flag-DN-p90RSK (MOI, 20) were exposed to Thb, and the SUMOylated MAGI1 (above the dotted line) and DN-p90RSK (below the dotted line) expression in the cells was assayed as described in Figure 5A. The data are representative of duplicate studies. *Nonspecific band. (**F**) HAECs pretreated with FMK-MEA (10 μM, 30 min) or a vehicle were exposed to Thb (10 U/mL for the indicated times. Total cell lysates were analyzed for p90RSK, c-Jun N-terminal kinase (JNK), p38, and ERK1/2 activation using Simple Western blotting with the Wes system (Proteinsimple) with anti-p-p90RSK, -p90RSK, -p-c-Jun N-terminal kinase, -c-Jun N-terminal kinase, -p-ERK1/2, -ERK1/2, -p-p38, and -p38 antibodies as described in the methods. The data are representative of duplicate studies.

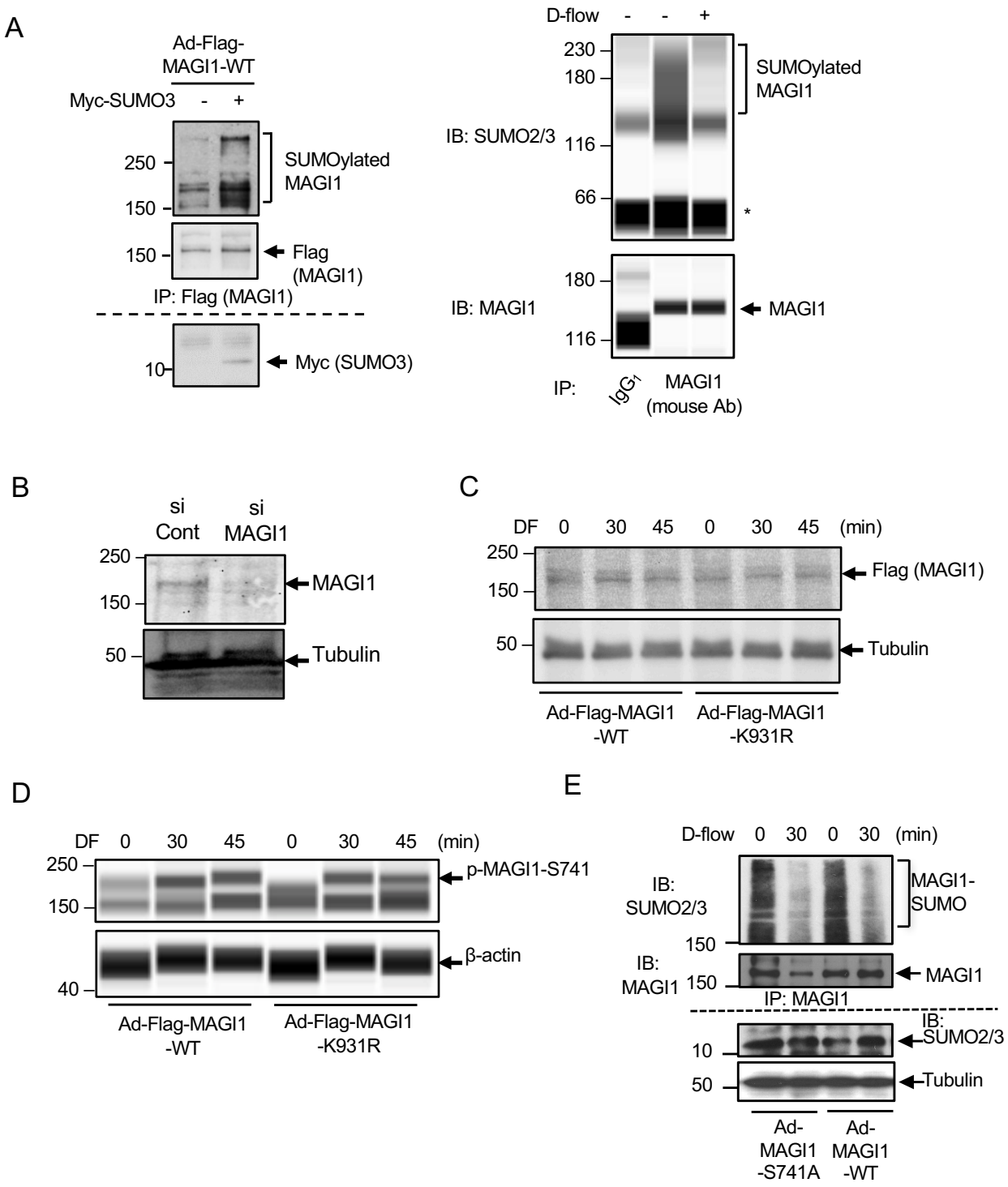

Supplemental Figure 4

Supplemental Figure 4. MAGI1 SUMOylation in ECs detected using Myc-tagged SUMO3 and the relationship between MAGI1 phosphorylation and SUMOylation. (**A, left**) HAECs were transfected with Flag-MAGI1-WT as well as a Myc-SUMO2/3 construct. Twenty-four hours after transfection, MAGI1 SUMOylation was assessed using IP with an anti-Flag antibody followed by IB with an anti-Myc antibody (first panel above line) and then with an anti-Flag antibody to confirm that equal amounts of MAGI1 protein were pulled down (second panel above line). The bottom panels show Myc-SUMO3 expression levels in the total cell lysates. The data are representative of duplicate studies. (**A, right**) HUVECs were exposed to d-flow for 20 min, and the level of SUMOylated MAGI1 expression in them was determined via IP with an anti-MAGI1 (mouse, Santa Cruz #SS-5) antibody and then IB with an anti-SUMO2/3 antibody with capillary electrophoresis western analysis as described in the Methods. (**B-E**) MAGI1 S741 phosphorylation (**B-D**) and SUMOylation (**E**) in ECs transduced with Ad-Flag–MAGI11-WT or -K931R (**C**, **D**) or -S741A (**E**). (**B-D**) Endogenous MAGI1 expression was depleted by siRNA treatment and confirmed by Western blotting (**B**). Then, adenoviral vectors encoding MAGI1 WT or K931R mutant were transduced into MAGI1 siRNA-treated cells. Western blot results confirm Ad-Flag-MAGI1-WT and K931R mutant expression (**C**). Cells were subjected to d-flow for indicated times and MAGI1-S741 phosphorylation was assessed using capillary electrophoresis Western analysis (**D**). The panels are representatives from three different experiments. (**E**) Ad-Flag–MAGI1-WT or -S741A was co-immunoprecipitated with anti-MAGI1 followed by IB with anti-SUMO2/3. The data are representative of duplicate studies. Adenoviral transduction: MOI, 20.

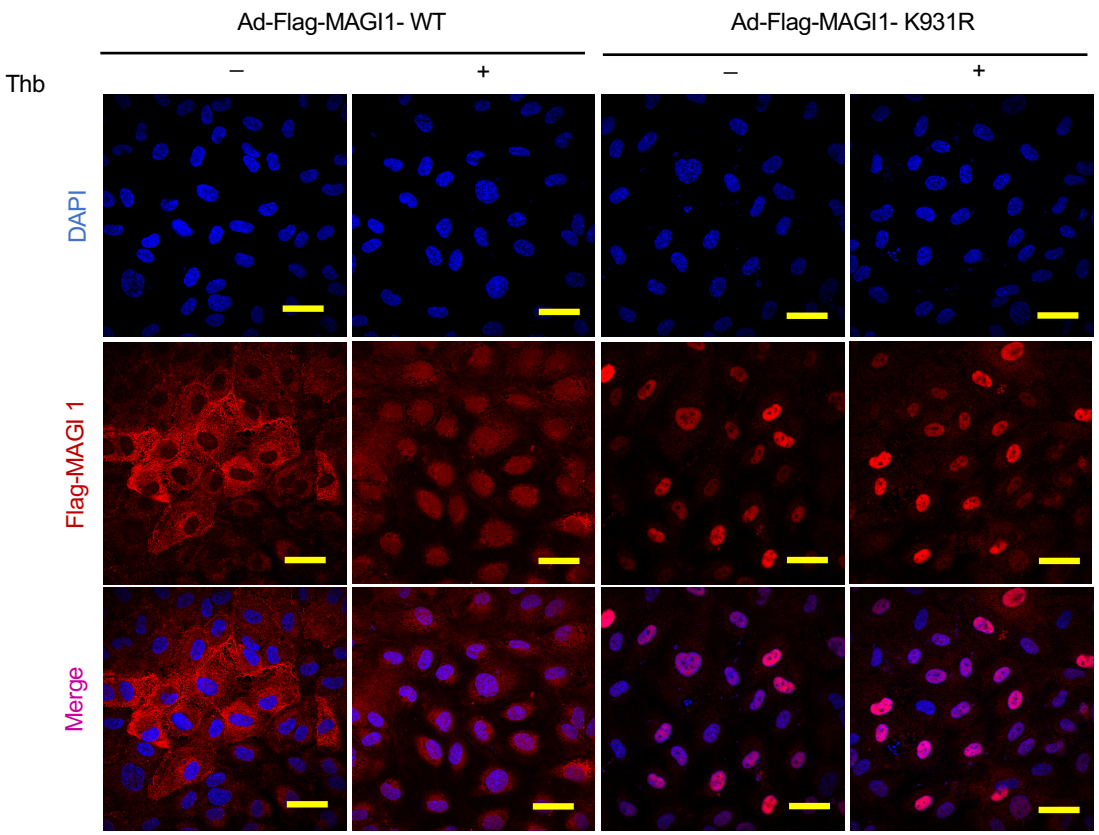

Supplemental Figure 5

Supplemental Figure 5. MAGI1-K931 deSUMOylation elicits nuclear translocation of MAGI1. Low magnification of the images shown in Figure 6A are presented. Scale bars, 20 μm

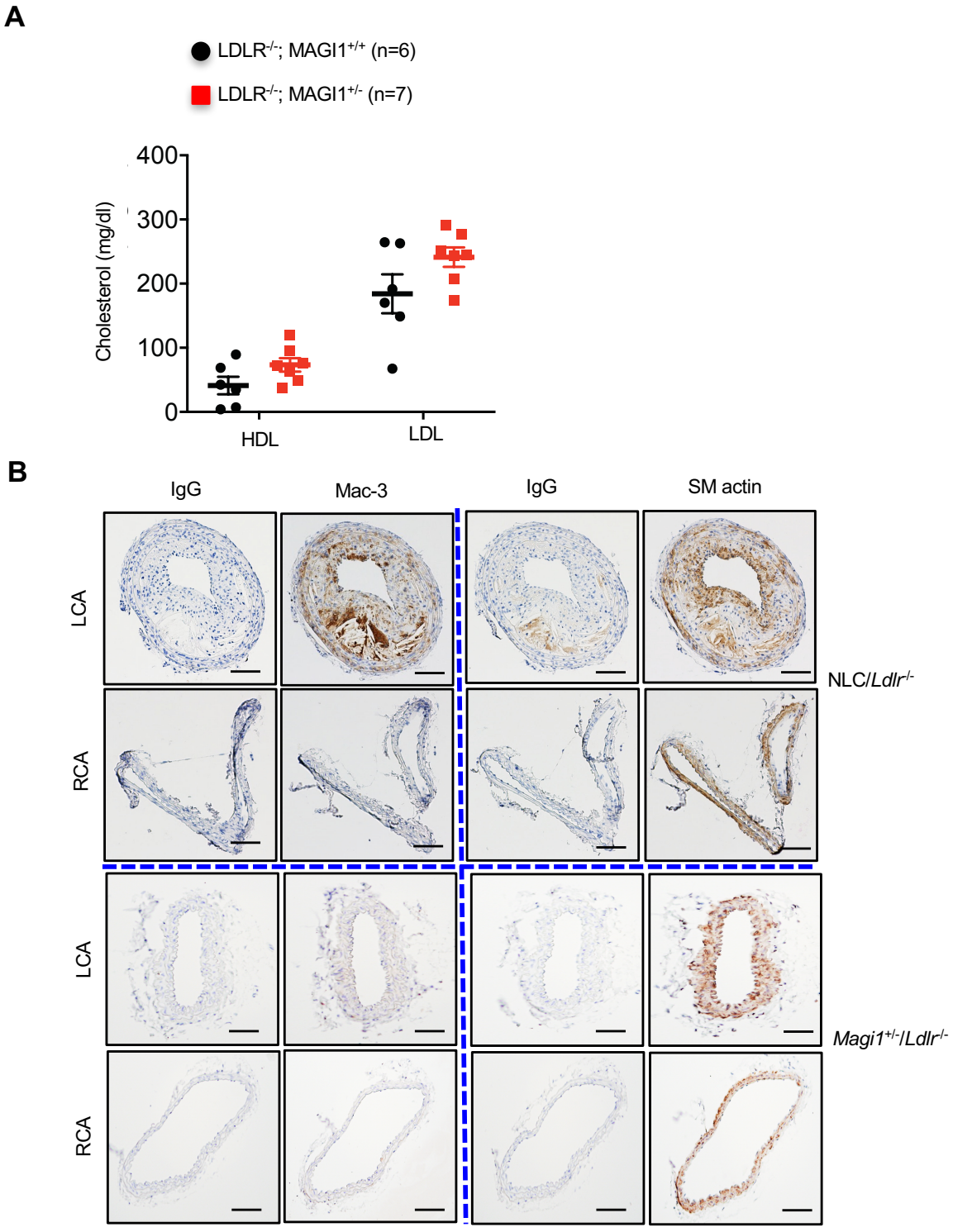

Supplemental Figure 6

Supplemental Figure 6. Cholesterol level and reduced macrophage infiltration into the atrosclerotic plaque in *Magi1*$^{+/-}$/*Ldlr*$^{-/-}$ mice. (**A**) HDL and LDL level in NLC/*Ldlr*$^{-/-}$ and *Magi1*$^{+/-}$/*Ldlr*$^{-/-}$ mice. The data are presented as mean ± SEM (n = 6-7). (**B**) LCA and RCA sections obtained in d-flow–induced atherosclerosis studies (Figure 7A) were immunostained with antibodies against Mac3 (macrophages) or α-smooth muscle actin (smooth muscle cells). These representative immunohistochemical images of Mac3 and α-smooth muscle actin staining of atherosclerotic lesions show that macrophages infiltrate intimal lesions in the LCA but not the RCA and that macrophage infiltration is reduced in *Magi1*$^{+/-}$/*Ldlr*$^{-/-}$ mice. Scale bars, 200 μm. *We have already reported significant macrophage and foam cell accumulation in LCA lesions in the PCL model[7,20], which represents atherosclerosis formation but not restenosis of lesions (which have very limited macrophage infiltration) after angioplasty. Therefore, this figure confirms that our model is an atherosclerosis model with significant macrophage infiltration as we reported previously[21]. We randomly chose three animals from each group of NLC/*Ldlr*$^{-/-}$ and *Magi1*$^{+/-}$/*Ldlr*$^{-/-}$ mice and confirmed significant macrophage infiltration in them, especially in NLC/*Ldlr*$^{-/-}$ mice after PCL.

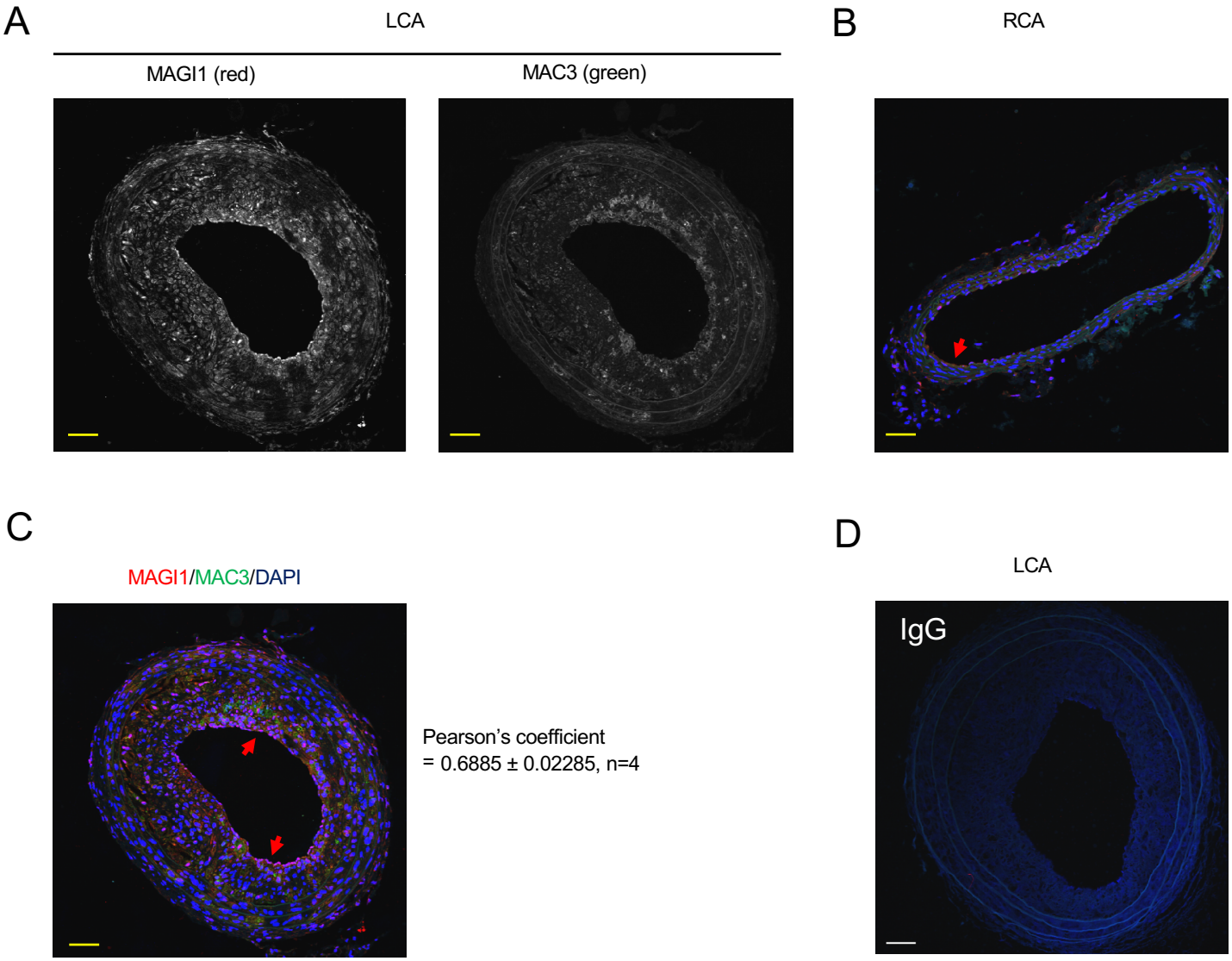

Supplemental Figure 7

Supplemental Figure 7. Co-localization of MAGI1 and macrophage staining in plaques after PCL. (**A-C**) LCA and RCA sections obtained in d-flow–induced atherosclerosis studies (Figure 7A) were stained with anti-Mac3 (macrophages, green) and anti-MAGI1 (red) and DAPI (blue). Confocal laser scanning microscopy was used to record images of the sections. Autofluorescence was not detected in the red channel. (**D**) A normal rabbit IgG was used as a negative control. Scale bars, 100 μm. (**C**) Co-localization of Mac3 and MAGI1 staining in LCA sections was assessed using Pearson's correlation coefficient as described in Methods. Data are presented as mean ± SEM. (**E** and **F**) Intensity of MAGI1 staining at the luminal surface (**E**) and medial layer (**F**) of the LCA and RCA as detected using ImageJ. Data are presented as mean ± SEM (n = 4/group). $^{**}p$ <0.01. N.S., not significant. (**G**) The intima:media ratios in hematoxylin- and eosin-stained LCA sections[7]. Data are presented as mean ± SEM for NLC/*Ldlr*$^{-/-}$ (n = 6) and *Magi1*$^{-/-}$/*Ldlr*$^{-/-}$ (n = 5) mice.

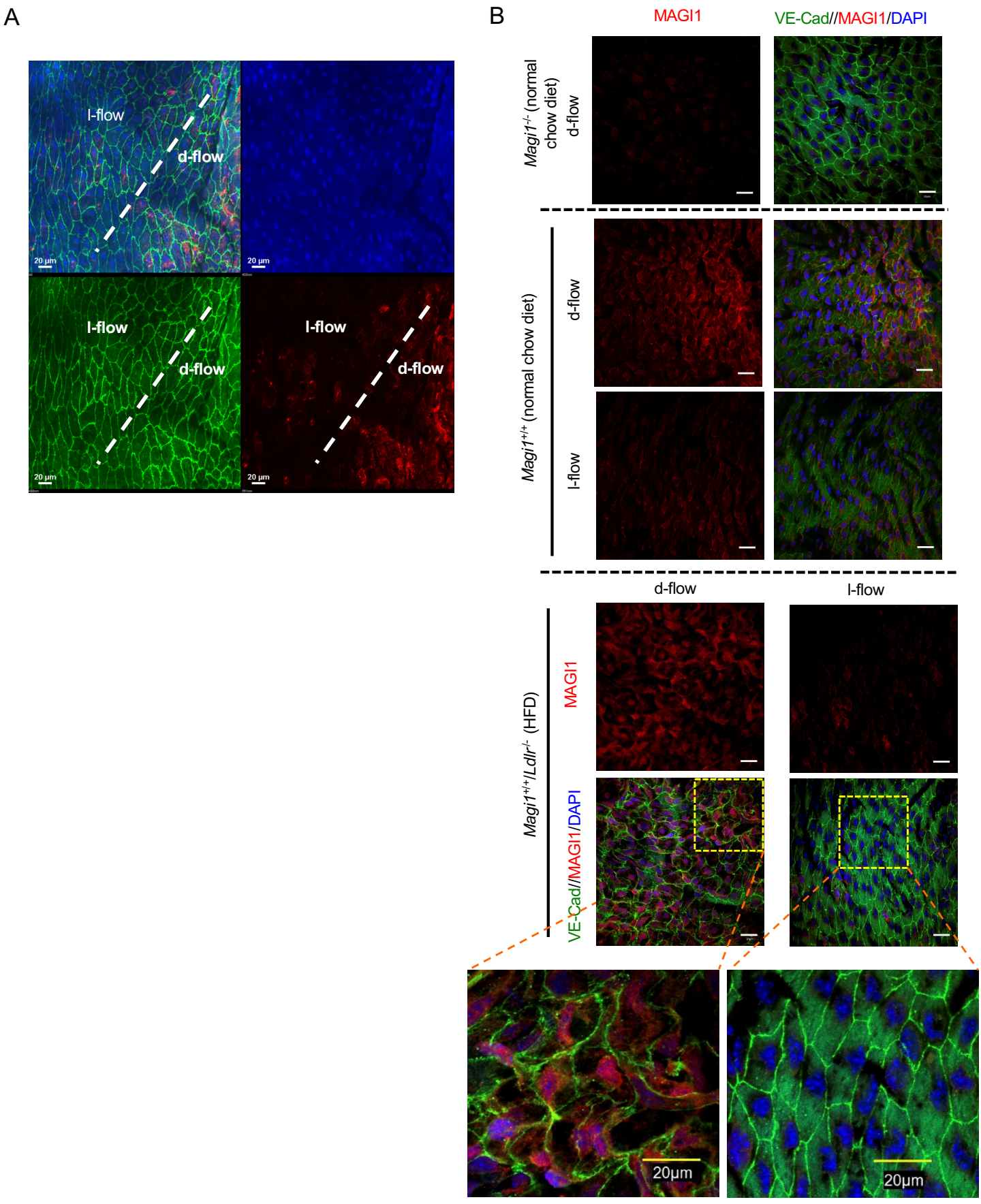

Supplemental Figure 8

Supplemental Figure 8. MAGI1 expression in d-flow and l-flow areas at the murine aortic arch. (**A**) *En face* preparations of aortas from *Magi1*$^{+/+}$ mice fed an NC diet were co-immunostained with anti-VE-cadherin (green) and anti-MAGI1 (red). Shown are border areas exposed to l-flow and d-flow. (**B**) Aortas were harvested from *Magi1*$^{-/-}$ (top panel) and *Magi1*$^{+/+}$ (second and third panels from the top) mice fed an NC diet and *Magi1*$^{+/+}$/*Ldlr*$^{-/-}$ mice (fourth and fifth panels from the top) fed an HFD. *En face* preparations of the aortas were co-immunostained with anti-VE-cadherin (green) and anti-MAGI1 (red). Shown are areas exposed to l-flow and d-flow. In ECs exposed to d-flow, MAGI1 expression was increased, and it was further upregulated in early atherosclerotic lesions in *Magi1*$^{+/+}$/*Ldlr*$^{-/-}$ mice fed an HFD. The boxed areas in the fifth panel are magnified at the bottom. Scale bar, 20 μm.

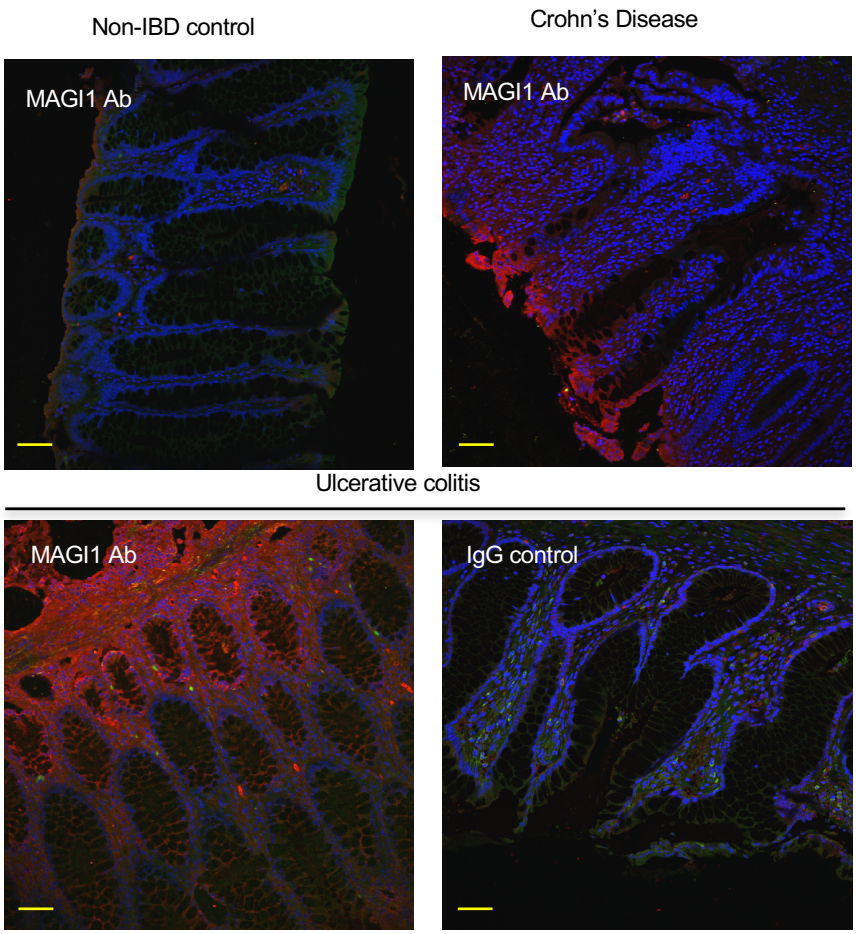

Supplemental Figure 9

Supplemental Figure 9. MAGI1 expression in human IBD samples. Paraffin-embedded sections of colonic tissues obtained from patients with ulecerative colitis or Crohn's disease and non-IBD controls were co-stained with anti-MAGI1 (red), anti-CD31 (green), and DAPI (blue). Confocal laser scanning microscopy was used to record images of the sections. Autofluorescence was not detected in the red channel. Increased MAGI1 staining at the luminal surface area was observed in these sections as shown in Figure 7g. Scale, 100 μm. Ab, antibody.

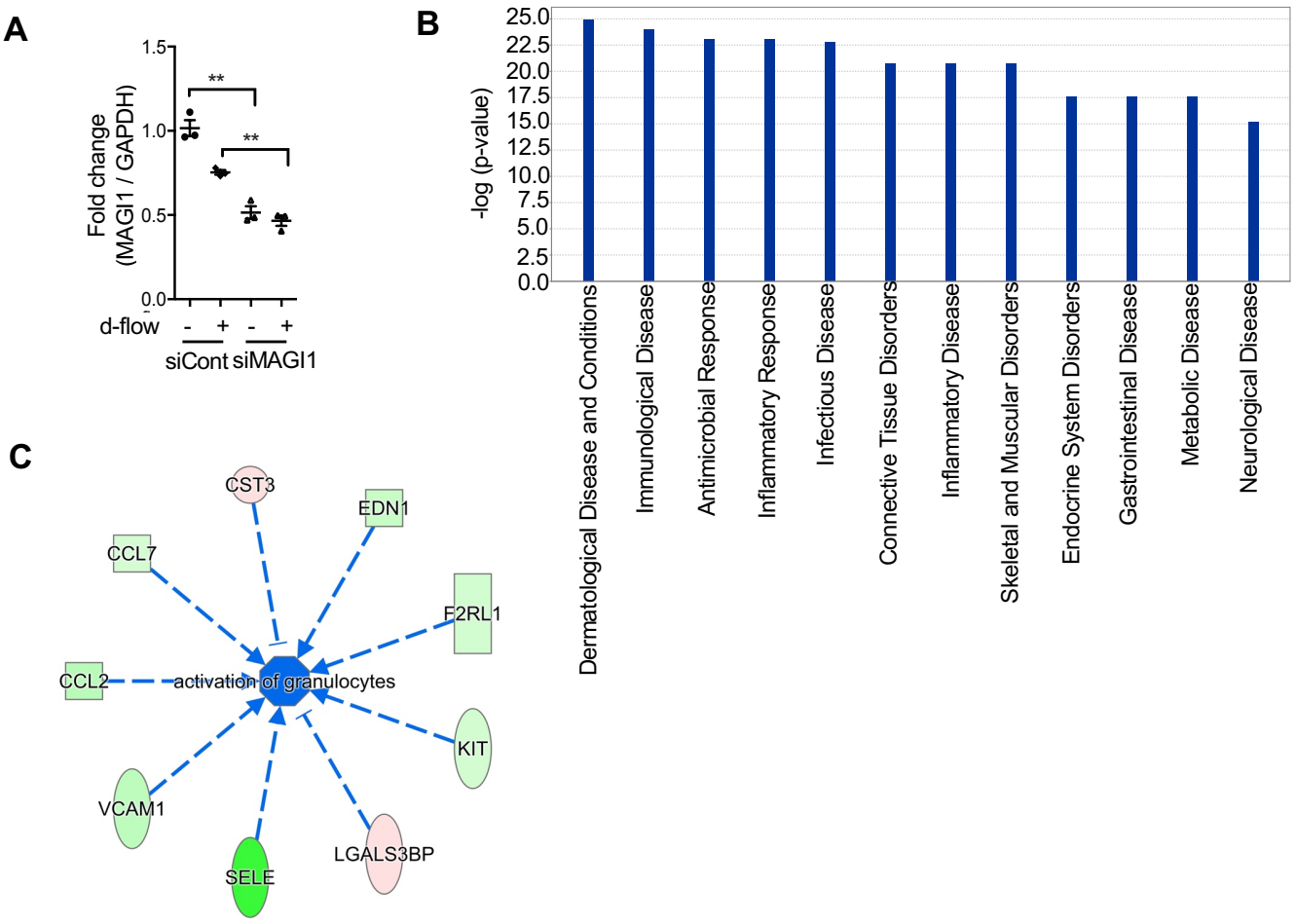

Supplemental Figure 10

Supplemental Figure 10. Enriched disease and biological functions detected by IPA analysis and classification of differentially expressed genes regulated by MAGI1 in response to d-flow. (**A**) The expression of *Magi1* in ECs with and without d-flow after treatment with MAGI1 siRNA (siMAGI1) or control siRNA (siCont) was quantified using qRT-PCR. Data are presented as mean ± SEM ($n = 3$). $^{**}p < 0.01$. Statistical differences were assessed using the one-way analysis of variance followed by Bonferroni post hoc testing for multiple group. (**B**) Statistical significance of IPA-determined biological functions and disease gene enrichment in MAGI1 siRNA-treated ECs calculated using a right-tailed Fisher exact test and presented as -log(*P*) values. A larger value on the y-axis represents greater significance. We found 491 genes that were differentially expressed in MAGI1 and control siRNA-transfected cells ($p < 0.05$; absolute fold change >2), with 386 upregulated and 105 downregulated genes in cells treated with MAGI1 siRNA. Gene expression profiles in d-flow–stimulated ECs with MAGI1 and control siRNA transfection were also analyzed using unpaired one-way analysis of variance with a statistical threshold of $p < 0.05$ and twofold change restriction to identify differentially expressed genes in the control and *Magi1* siRNA-transfected cells stimulated by d-flow. We identified 592 genes as being differentially expressed under d-flow stimulation and classified them further based on their biological functions using Ingenuity Downstream Effects Analysis (QIAGEN). Dermatological Disease and Conditions, Immunological Disease, Antimicrobial Response, Inflammatory Response, and Infection Disease were the five most significant changes (-log[*P*] >20) disease and biological function categories. The *p* values, calculated using the Fisher exact test, reflects the likelihood that the association between a set of genes in our data set and a related biological function is significant. (**C**) The reduction of the "activation of granulocytes" function predicted using IPA Downstream Effect Analysis. In the Inflammatory Response category, the downstream effects analysis predicted the reduction of this function. This network displays all the genes with defined significant differential expression associated with activation of granulocytes based on published findings in the Ingenuity Knowledge Base. CCL7 and CCL2, chemokine (C-C motif) ligands 7 and 2; KIT, KIT proto-oncogene receptor tyrosine kinase; EDN1, endothelin 1; SELE, E-selectin; LGALS3BP, lectin, galactoside-binding, soluble, 3-binding protein; F2RL1, lectin, galactoside-binding, soluble, 3-binding protein (also known as PAR-2); CST3, cystatin C. Green indicates genes with decreased expression, red indicates genes with increased expression, and blue indicates a predicted decreased effect on the "activation of granulocytes" function based on published findings of a gene's effect together with a gene's expression change.

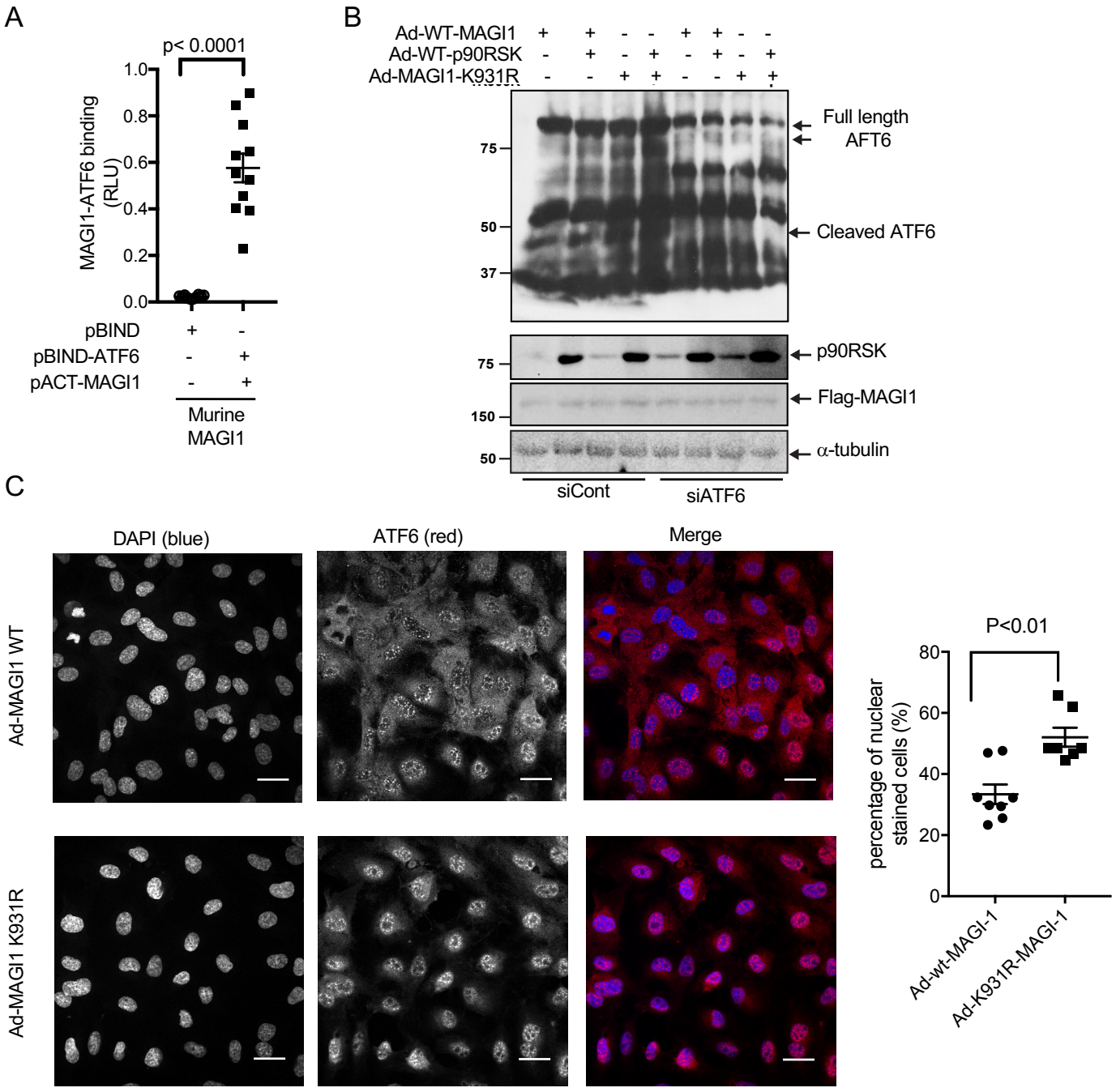

Supplemental Figure 11

Supplemental Figure 11. Nuclear translocation of the MAGI1-ATF6 complex.
(**A**) MAGI1-ATF6 binding was assessed using a CheckMate Mammalian Two-Hybrid assay. HAECs were transfected with murine pACT-MAGI1-mouse, pBIND-ATF6, or a luciferase reporter vector (PG5-Luc), and their luciferase activity was measured. Relative MAGI1-ATF6 binding data are presented as firefly:Renilla luciferase activity ratios (n = 11-12). P value shown in figure. Data are presented as mean ± SEM. RLU, relative light units. (**B**) HUVECs were treated with ATF6 or control siRNA for 48 h and transduced with an adenovirus containing WT p90RSK (Ad -p90RSK-WT), MAGI1-WT (Ad -MAGI1-WT), or the MAGI1-K931R mutant (Ad-MAGI1-K931R). p90RSK, MAGI1, and ATF6 expression were detected using Western blotting as indicated. (**C**) HUVECs were transduced with Ad-Flag-MAGI1-WT or -K931R and then immunostained with anti-ATF6 (red) and DAPI (blue). ATF6 staining was cytoplasmic in cells transduced with Ad-Flag-MAGI1-WT but nuclear in cells transduced with Ad-Flag-MAGI1-K931R. The percentage of cellular ATF6 localization in the HUVECs is quantified in the graph at right. Data are presented as mean ± SEM. Statistical differences between two independent groups were assessed using the Student t-test (two-tailed).